

Journal Pre-proof

Vulnerability of bridges to individual and multiple hazards- floods and earthquakes

Sotirios A Argyroudis , Stergios Aristoteles Mitoulis

PII: S0951-8320(21)00116-2
DOI: <https://doi.org/10.1016/j.ress.2021.107564>
Reference: RESS 107564



To appear in: *Reliability Engineering and System Safety*

Received date: 19 November 2020
Revised date: 16 January 2021
Accepted date: 18 February 2021

Please cite this article as: Sotirios A Argyroudis , Stergios Aristoteles Mitoulis , Vulnerability of bridges to individual and multiple hazards- floods and earthquakes, *Reliability Engineering and System Safety* (2021), doi: <https://doi.org/10.1016/j.ress.2021.107564>

This is a PDF file of an article that has undergone enhancements after acceptance, such as the addition of a cover page and metadata, and formatting for readability, but it is not yet the definitive version of record. This version will undergo additional copyediting, typesetting and review before it is published in its final form, but we are providing this version to give early visibility of the article. Please note that, during the production process, errors may be discovered which could affect the content, and all legal disclaimers that apply to the journal pertain.

© 2021 Published by Elsevier Ltd.

Highlights

- Novel fragility models for scoured-critical bridges exposed to multiple hazards were generated
- Rigorous FEM included the water-soil-bridge interaction under flooding and earthquakes
- Failure modes for bridge components exposed to floods were described
- Insights on the flood vulnerability of integral and bridges with bearings are provided
- Consideration of uncertainties in scour formation enhance the reliability of risk assessment

Journal Pre-proof

Vulnerability of bridges to individual and multiple hazards- floods and earthquakes

Sotirios A Argyroudis¹, Stergios Aristoteles Mitoulis²

¹Dpt. of Civil and Environmental Engineering, Brunel University, London, UK

²Dpt. of Civil and Environmental Engineering, University of Surrey, UK

Abstract

Building resilient bridges, capable of withstanding multiple natural stressors with minimal damage and quickly restore functionality is paramount to delivering climate-resilient transport infrastructure. Nevertheless, bridges are proven to be vulnerable to natural hazards, with flooding and earthquakes being the main causes of failure. The available research and practice for assessing the vulnerability of river-crossing bridges is predominantly qualitative and therefore relies heavily on visual inspections, while ignoring important characteristics of the complex water-soil-bridge interaction. This is a knowledge gap that this paper aims to fill. This work provides novel fragility models for hydraulically induced stressors and/or combinations of hydraulic and seismic hazards. To achieve this, unique detailed two- and three- dimensional numerical models are employed, for a typical three-span prestressed box-girder river-crossing bridge. This paper is a primer on the vulnerability of flood-critical bridges as it models the entire water-soil-bridge system, taking into account critical hydraulic stressors (scour, debris accumulation, hydraulic forces), the uncertainty in scour hole formation, and all components of integral and isolated bridges: deck, bearings, piers and abutments, backfill, and the foundation soil. A detailed description of the damage modes for each component is given and sets of fragility curves for floods and combinations of hydraulic stressors and earthquakes are developed. The study concludes that integral bridges are in most cases more vulnerable to local scour than bridges with bearings, since the latter are more flexible and can therefore adapt to changes in their geometry. The opposite is true for global scour and/or seismic earthquake excitations. The generated fragility models are useful tools for quantitative risk assessment of transport systems and provide practical means in resilience-based asset management by owners and operators of transport infrastructure.

Keywords: bridge; flood; scour; earthquake; fragility; failure modes; numerical modelling

1. Introduction

Bridges are key assets of the transport infrastructure upon which the world's economies and societies are highly dependent. Road and rail bridges are vulnerable components of transport networks that are exposed to multiple hazards worldwide (Koks et al., 2019), and their failure can have a significant impact on the functionality of the transport system. Ageing effects increased traffic loads and natural hazards, such as earthquakes, heavy rainfall, floods or extreme temperatures, which are expected to intensify due to changes in global climate (Dikanski et al., 2018; Nasr et al., 2019; Nasr et al., 2020), can hamper the safety and continuous operation of bridges. In particular, closure of river-crossings can lead to severe network disruption, due to very limited or no diversion alternatives, taking into account that more than one bridge may fail in the same region, along a river, during an extreme event. In this respect, flood-induced scour was identified as the predominant cause of bridge failure (Briaud et al., 2014; Wardhana and Hadipriono, 2003). Several failures have been reported as a result of hydraulically triggered scour and debris accumulation as for example in the USA (Cook et al., 2015), the United Kingdom (Mathews and Hardman, 2017; Panici et al., 2020), Italy (Scozzese et al., 2019), Serbia (Tanasic and Hajdin, 2018) or more recently in Greece (Zekkos et al., 2020). A

recent workshop (Lamb et al., 2017) also revealed that the damage to bridges is strongly related to their scour history. Therefore, undetected scour with bridge low redundancies can lead to abrupt and unexpected failures after floods of lower intensity or when permanent scour is combined with other hazards, such as earthquakes. Scour history imposes great uncertainties, which in conjunction with potentially unknown foundation depth, history of debris accumulation, number of floods in the last five years and whether the bridge characteristics are well known, may lead to increased vulnerability. Also, climate change has increased the frequency and intensity of severe weather events (IPCC, 2014) and led to sea-level rise, including storm surges in coastal areas (Vousdoukas et al., 2018). Climate change, therefore, exacerbates the corrosion of structures, the erosion of the surrounding soil and the occurrence of severe events, such as flash floods. Thus, the increased vulnerability of bridges under multiple hazard stressors including climate change uncertainty, poses a major challenge for transport infrastructure operators, seeking a more robust and resilient infrastructure (Mondoro et al., 2018; Akiyama et al., 2019; Liu and Song, 2020). So far, very few studies have addressed the impact of climate change and multiple hazard effects on the resilience of bridges (Dong et al., 2013; Decò et al., 2013; Dong and Frangopol, 2015; Banerjee et al., 2019; Argyroudis et al., 2020a; Li et al., 2020). Yet, there is very sparse research on the fragility modelling of flood-critical bridges.

The robustness of a transport asset to hazard actions is commonly quantified using fragility functions, which give the probability of the asset exceeding defined damage states, for a given hazard intensity, e.g. peak ground acceleration for earthquakes, water discharge or scour depth for floods. There has been extensive research on the development of numerical fragility functions for bridges exposed to individual hazards, with the majority of studies focusing on seismic effects (e.g. Nielson and DesRoches, 2007; Billah and Alam, 2015; Karamlou and Bocchini, 2015; Stefanidou and Kappos, 2019; Shekhar and Ghosh, 2020). The vulnerability of bridges to flood effects has been investigated by limited studies, including those by Kim et al. (2017), Hung and Yau (2017) and Ahamed et al. (2020).

The fragility analysis for multiple hazards is a relatively new area of research, yet, of utmost importance as multiple stressors reduce the capacity and functionality of bridges and transport networks (Li et al., 2011; Bruneau et al., 2017; Gidaris et al., 2017; Argyroudis et al., 2019). Most of the available studies focus on the combined scour and seismic effects based on numerical modelling (Banerjee and Prasad, 2013; Prasad and Banerjee, 2013; Wang et al., 2014; Kameshwar and Padgett, 2014; Guo et al., 2016, 2019; Yilmaz et al., 2016; He et al., 2020). The combined effect of flood and earthquake hazards is commonly visualised with fragility surfaces (Yilmaz et al., 2016; Guo et al., 2016), which provide the failure probability of the bridge as a function of the corresponding intensity measures. The most common approach to simulate scour effects is the removal of equivalent soil springs, corresponding to the resistance of the soil around the piles or shallow foundation, which has been washed away during floods. This removal reduces the lateral stiffness and load-bearing capacity of the foundation and changes the dynamic behaviour of the soil-structure system (Tubaldi et al., 2019). In some instances, a more accurate approach is adopted, where the stiffness of the soil springs is varied to take into account the change in soil stresses and water pressures due to scour formation (He et al., 2020). However, this is a simplified approach that neglects the impact of scour geometry and the change in soil properties due to saturation and scour formation, as well as the various sources of damping within the soil and the inertia and kinematic interaction during an earthquake. Other simplified approaches include, e.g. the study by Tanasic and Hajdin (2018), who estimated the damage probability for bridges considering degradation criteria of soil parameters over time due to scouring, and failure criteria on the basis of geotechnical, i.e. settlement, or structural, i.e. excess of deck ultimate capacity, failure mechanisms. It is established that these simplistic approaches provide valuable information, nevertheless, omit important parameters that influence the behaviour and thus the fragility of the complex water-soil-bridge system. This is another fundamental gap in the scientific knowledge that this paper tries to fill.

The main objective of this paper is to provide a framework for the fragility analysis of bridges under single and combined multiple hazards, based on detailed numerical modelling of bridges exposed to flood effects (scour, hydraulic forces and debris accumulation) followed by seismic shaking. Flood-induced failure modes

are identified and described in detail, and fragility curves are produced considering different combinations of scouring conditions and earthquake loadings. Fragility curves are generated for the components (e.g. deck, pier, abutment) and the system, i.e. bridge, while fragility surfaces are also produced for combined hazards. For the first time in the international literature, fragility curves are developed for scour-critical reinforced concrete bridges with shallow foundations, taking into account the full interaction between the bridge, the soil and the water. This type of foundation is most typical for bridges constructed in the 1960s and 1970s, which make up the majority of our transport networks, among which masonry bridges are said to be the most vulnerable ones (Scozzese et al. 2019). This makes them more vulnerable to natural hazards in comparison with their counterparts with deep foundations, and their vulnerability is greater due to deterioration and increased traffic loads as well as due to lack of relevant design regulations. Another novelty of the paper is that the entire 3D model of the bridge has been simulated, including the foundation, piers, bearings, deck, abutments, backfill and foundation soil, enabling a more holistic evaluation of bridge performance. The model included the non-linear behaviour of the soil, by cluster elements, which allowed the identification of the evolution of scour formation and the gradual loss of the contact between the foundation and the soil, the changes of the soil properties during the analysis, as well as recording of the compatible displacements of the settling bridge and the resulting evolution of bridge internal actions, i.e. bending moments, shear, axial forces, drifts etc. For the first time, a considerable effort was put into modelling realistic geometries of the scour hole, both upstream and downstream, longitudinally and transversally to the bridge shallow foundations, to achieve an understanding of the temporal and spatial variability of the scour effects. This paper thus provides further advancement in the quantitative risk analysis of flood critical transport assets (Lounis and McAllister, 2016; Pregolato, 2019) and the resilience assessment at asset and system level for multiple hazards (Ayyub, 2014; Woods, 2015; Achillopoulou et al., 2020). In this respect, the generated fragility models are expected to provide reliable and efficient tools to infrastructure owners and network operators, who are increasingly faced with the challenge of understanding and evaluating the risks of bridges and transport networks (Lamb et al., 2019; Argyroudis et al. 2020b). Ultimately this paper underpins the delivery of more resilient infrastructure by adapting capacities and functionalities to multiple hazard stressors, exacerbated by climate change.

2. Multihazard fragility analysis for bridges

The flowchart of the proposed framework for the generation of numerically based fragility functions for river-crossing bridges exposed to combined flood (FL) and earthquake (EQ) hazard effects is shown in Figure 1 and comprises the following six main steps. The process and flowchart are focusing on concrete, steel and composite bridges; however, it can be readily adopted in masonry bridge assessments after considering certain modifications, e.g. bridge properties in step i, or different EDPs and damage state definitions in step ii.

Step (i) Definition of the bridge properties, which includes a three-span prestressed bridge with its components, i.e. continuous box girder deck, wall-type abutments and piers, shallow foundations, backfills and foundation soil. Two types of abutment and pier-deck connections are considered, i.e. monolithic and through elastomeric bearings. **Step (ii) Engineering demands parameter (EDP) and definition of damage states for each component** (see also Table 1). These include the maximum bending moment for critical sections of the deck, pier and abutment, the displacement/drift of piers and abutments, the settlement of the footing and the backfill, and the axial and shear displacements of the bearings. The damage states, also known as limit states, i.e. minor, moderate, extensive and complete, are defined for each component based on the range of EDPs values, as defined in Table 2. **Step (iii) Definition of hazard actions and intensity measures (IM)**. FL effects due to river flows are distinguished to global, i.e. rise in water level and global scouring of the river bed, and local, i.e. formation of a scour hole under the footing(s), hydraulic forces acting on the pier(s), and accumulation of debris at pier(s) upstream. A progressing scour depth is analysed. Each scour depth corresponds to a given water discharge, Q and flow depth, y_0 , based on the literature (Arneson et al., 2012; Pizarro et al., 2020), accounting for the characteristics of the river and the water flow. Different scour

geometries and combinations of scour hole locations are employed, as described in section 4. For the EQ hazard, acceleration time histories were selected as outcrop motion for the analyses, scaled to different intensities. The IM used for the earthquake hazard is the Peak Ground Acceleration (PGA). The seismic analysis is performed for each scour depth, to simulate the random combination of the two hazards. Figure 1 provides hazard IM and range of values used in this paper, yet, different values might be considered by the assessor. **Step (iv) Numerical model.** A FEM was created in Plaxis 3D (2019) considering its capabilities and the needs of this investigation. Specifically, the study required modelling the FL effects described in step (iii) and to take into account the interaction between the different structural components of the bridge and the interaction of the latter with the foundation and the water. In this way, a number of unique 3D models were generated, where the soil is modelled with cluster elements, as opposed to the most common modelling with soil springs. The Mohr-Coulomb criterion was adopted for the soil, while the scour effect was modelled by gradually removing soil elements around and under the foundation, reaching the maximum scour depth, as per Figure 6. For the multihazard FL-EQ analysis, a 2D model was employed to facilitate the computationally demanding time-history analyses. In this case, the seismic input was uniformly applied at the basis of the model for different combinations of scour, i.e. pier only, abutment only, pier and abutment. The numerical models are described in section 4. **Step (v) Evolution of damage:** For each component of the system and each hazard scenario, the EDPs are plotted against the selected IM on a logarithmic scale and a regression curve is fitted (McKenna et al., 2020). **Step (vi) Multihazard fragility functions:** The fragility parameters are defined and the fragility curves/surfaces are generated for each component (see section 5). The median IM is obtained for each damage state using the regression models of step (v) and the definitions of the damage states (step ii). The total variability (β_{tot}) comprises three sources of uncertainty. The one associated with the definition of limit states (β_{LS}) was taken 0.35, while the uncertainty due to the capacity (β_C) has been estimated at 0.35 (Argyroudis et al. 2019). The third uncertainty is associated with the hazard demand and is calculated by the dispersion in response to the variability of hazard actions and their combinations, i.e. based on the residuals of the calculated EDPs against the best fit in step (v). The combined effect of the two hazards is illustrated by fragility surfaces for each component, as well as for the entire bridge system, assuming components in a series connection (Stefanidou and Kappos, 2017; Ghosh and Sood, 2016).

This framework has been applied using the cumulative distribution function (CDF) for estimating the fragility of the bridge as per Gidaris et al. (2017) and Ghosh and Padgett (2010). Bridge system fragility has multiple failure modes, and hence, can be also estimated by solving a reliability problem that involves structural capacities of the components and the corresponding hazard induced demands as described in Gardoni et al. (2002, 2003) based on point estimates of fragility. The latter is a more accurate and representative approach as well as more adaptable, because physics-based fragility functions can embrace experimental or field data to improve the accuracy of fragility models. However, the objective of this paper is broad and as a result it includes a large number of parameters, such as EDPs, and hazard stressors and a number of structural and geotechnical components. Hence, the Gardoni et al. (2002, 2003) approach would be computationally very tedious and can be applied in future research endeavours. Furthermore, this paper is focused on a prestressed concrete bridge with surface foundations and future research will include deep foundations, other components and bridge types and well-informed EDPs, by utilising for example monitoring data (Achilopoulou et al. 2020). Also, further developments can incorporate results from sensitivity analysis, where different hydraulic parameters, river properties and diverse earthquakes can be assessed on the basis of the bridge vulnerabilities.

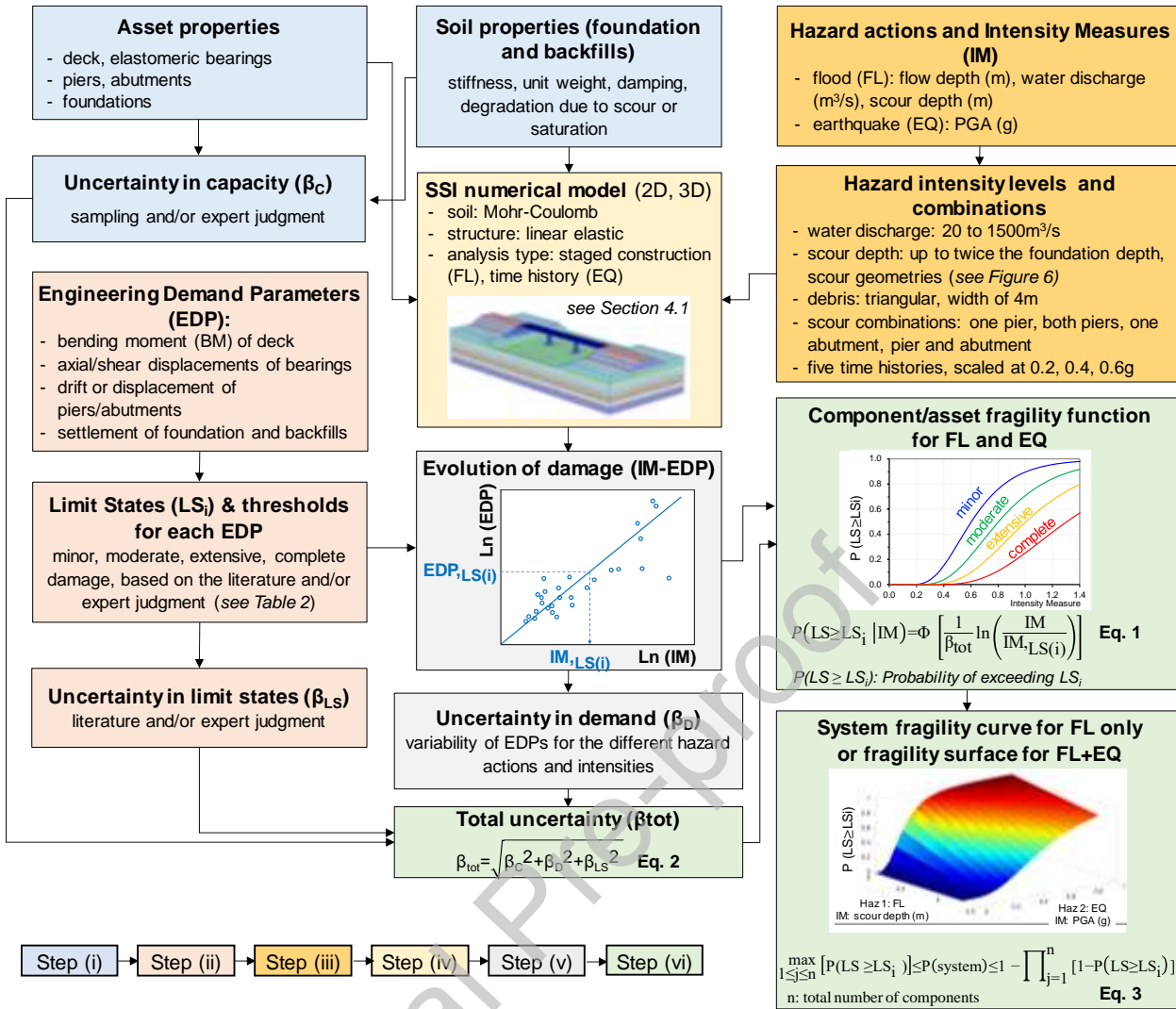


Figure 1. Flowchart for fragility functions of bridges exposed to flood (FL) and earthquake (EQ) hazards.

3. Failure modes due to flooding

Based on the analysis of 36 case studies of hydraulically induced bridge failures, Lin et al. (2014) found that local scour is the dominant cause (64%), followed by channel migration (14%) and contraction scour (5%). Most scour depths (i.e. up to 41%) ranged from 0.5 to 5.0 m, while the maximum scour depth was up to 15 m. To date, however, the extent of scouring that can trigger failure has not been sufficiently defined. Pier failure was the most common type (61%), followed by abutment failure (19%). Failure modes due to scour included vertical failure, lateral failure, torsional failure, and bridge deck failure. Most of the failures investigated were associated with lateral failure. Possible failure mechanisms due to scour effect are summarised by May et al. (2002) including structural movements or failures of the piers, abutments and footings and the superstructure/deck.

One of the main challenges in understanding the failure modes of flood-critical bridges is the crucial interaction between water-soil and the bridge. Some of the bridge components are directly affected, e.g. the foundation can be scoured, and hydraulic forces can be exerted on the footing, the pier and/or the abutment. In extreme cases, the high inundation depth can cause the water overtopping the deck, thereby exerting large hydraulic forces on the superstructure. These are primary effects. In other cases, an affected structural

component, for example, the foundation, might propagate movements and damages to other structural components, which are connected to the foundation, and thus, indirectly affect the entire system. These are secondary effects, influenced by hydraulic actions but they are only caused due to the compatibility displacements, which are indirectly imposed on the bridge components. The latter can lead to sequential failure propagation, e.g. failure of bearings due to pier settlements, which induce damage and movement to the deck and propagate damage to other components, e.g. other piers, abutments and backfills. The analysis of the effects of flooding on the foundations is therefore only a partial assessment and cannot provide an accurate estimate of the fragility and risks of the entire bridge system. To fill this gap, this paper, and on the basis of an extensive literature review and engineering assessment, proposes the failure modes presented in Table 1, while an illustrative and quantitative description of these failure modes is given in Mitoulis et al. (2021).

This table shows the primary and secondary effects of flood stressors on bridges. The first column shows the component that affected by the hazard stressor, e.g. the foundation soil and the pier, the second column shows the failure type, which is characterised as geotechnical (GEO) and structural (STR). The third and fourth column show the potential primary, i.e. direct effects, and secondary, i.e. indirect effects, correspondingly. Column (5) shows the bridge type that can be affected, e.g. if the bridge has deep or shallow foundations, or if it has bearings or has integral abutment and/or piers. The last column shows representative EDPs, e.g. settlement for the foundation and drift ratio for the pier or abutment.

Figure 2 shows sketches of potential damages for the three-span integral bridge caused only by scouring. Figure 2a shows the case where a bridge pier settles, with a uniform displacement downwards of $u_{p1,z}$. This displacement will possibly lead to the formation of two hinges (damage on both sides of the pier). These damages are expected to form within the deck, where the stresses due to bending moments (BM) change drastically, as shown in Figure 3, which is explained in more detailed below. Figure 2b illustrates the case where both piers of the three-span bridge are settling with displacements of $u_{p1,z}$ and $u_{p2,z}$. Based on expert judgement, it can be expected that hinges will be formed in all spans along the deck of the bridge, with critical positions F to E shown in Figure 3. Figures 2c and 2d show the cases where either only the abutment or both the abutment and the pier settle, which leads to the formation of hinges, i.e. damage within the first or second span and above the pier as per Figure 2d. All these figures are indicative, as these settlements can be either uniform or differential (longitudinally or transversally toward the upstream of the river). Also, these sketches do not show in three dimensions the potential influence of hydraulic forces and their exacerbation due to debris accumulation on the piers and/or at the abutments. Sketches of these potential damages are shown in Figure 4.

Table 1. Failure modes per bridge component, and description of primary and secondary effects and relevant EDP.

component (1)	failure type (2)	primary/direct effect (3)	secondary/indirect effect (4)	bridge type (5)	EDP (6)
foundation soil	GEO	scour hole, erosion, removal of sediment	settlement, bearing exceeded	all types	settlement
deep foundation	GEO & STR	tilting, buckling, cracking, yielding of piles	pull out of piles, damage by hydraulic loading, possibly aggravated by debris accumulation	bridges with deep foundations	pile yielding BM, including buckling/2nd order effects, pile cap failure (BM, SF), rotation, cracking width
shallow foundation	GEO & STR	settlement, concrete shear failure, flexural failure of reinforcement	damage by hydraulic loading, possibly aggravated by debris accumulation	bridges with shallow foundation	uniform and/or differential settlement, BM and/or SF, rotation, cracking width

backfill & approach slab	GEO	settlement, scour, erosion of the backfill	damage of the approach slab	all types	settlement
abutment & wing walls	STR & GEO	abutment settlement, abutment tilting or overturning, concrete cracking, reinforcement yielding	damage to wing walls	all types	drift ratio, yielding BM, cracking width
pier	STR	pier settlement/sinking, pier tilting (top or bottom rotation of the pier), damage by hydraulic loading, possibly aggravated by debris accumulation	concrete cracking, reinforcement yielding, overturning of the pier	all types with more than two spans	drift ratio, tilting, yielding BM, cracking width
deck	STR	deck damaged by collision of debris, and overtopping	due to pier/abutment movements: concrete cracking, reinforcement yielding, formation of hinges, prestressing failure (redistribution of stresses), span unseating and or permanent movements/dislodgement	all types	yielding BM, cracking BM, permanent deflection
bearings	STR	debris blockage	shearing, additional tension/compression permanent displacements, cavitation	isolated bridges	shear and axial (compressive or tensile) strains, rotation and combinations

GEO: geotechnical, STR: structural, BM: bending moment, SF: shear force

The damage shown in Figure 2, corresponds to the changes in the bridge geometry and the consequent alteration of stresses within the deck due to the settlements of the vertical supports, i.e. the piers and the abutment, caused by scouring. Figure 3(i) shows a typical continuous deck with its prestressing tendon profile. The same figure shows the positions where the tendon passes from the neutral axis (positions C and D), and the positions where the tendon has its maximum eccentricity downwards, in the middle of the span (A and H) and upwards at the supports (B and E). Figure 3(ii) shows a typical envelope of the BM diagrams for a continuous deck, where only vertical loads, i.e. self-weight, additional permanent load and traffic loads are exerted on the deck. Figure 3(iii) shows the elastic line of the deck when the abutment settles. Figure 3(iv) shows the additional BM due to the abutment settlement. The combination of this BM, with the envelope of BM in Figure 2(ii), gives the final BM. It is noted that the original bridge would have been designed for the envelope shown in Figure 3(ii) and therefore these additional BM of Figure 3(iv) are those expected to cause cracking and hence damage within the deck. It is also emphasised that prestressed decks are non-ductile structural components with very small tolerances to constraint vertical displacements. Small movements can lead to significant changes in the stresses, impacting SLS design situations and causing cracks within prestressed sections, directly affecting the serviceability and therefore the durability of the deck. In particular, Eurocode 2-Part 2, prohibits any cracking and for class 1 members, also tension is not allowable. Therefore, throughout the analysis of this paper, the stresses in all deck sections (F to E), have been continuously monitored as these are the actionable performance indicators, i.e. the EDPs (see section 4). This is because changes in stresses are not predicted during the design and therefore the prestressing tendons shown in Figure 3(i) are not designed for the occurrence of pier settlement. Similarly, the concrete of the prestressed deck is not expected to receive tension, yet, the changes in the geometry as described by Figures 2 and 3 could generate tension in the lower fibre at midspans and in the upper fibre at supports of continuous decks. Finally, Figure 3(v) shows the elastic line of the three-span deck, where the pier settles, and Figure 3(vi) illustrates the additional BM due to this settlement.

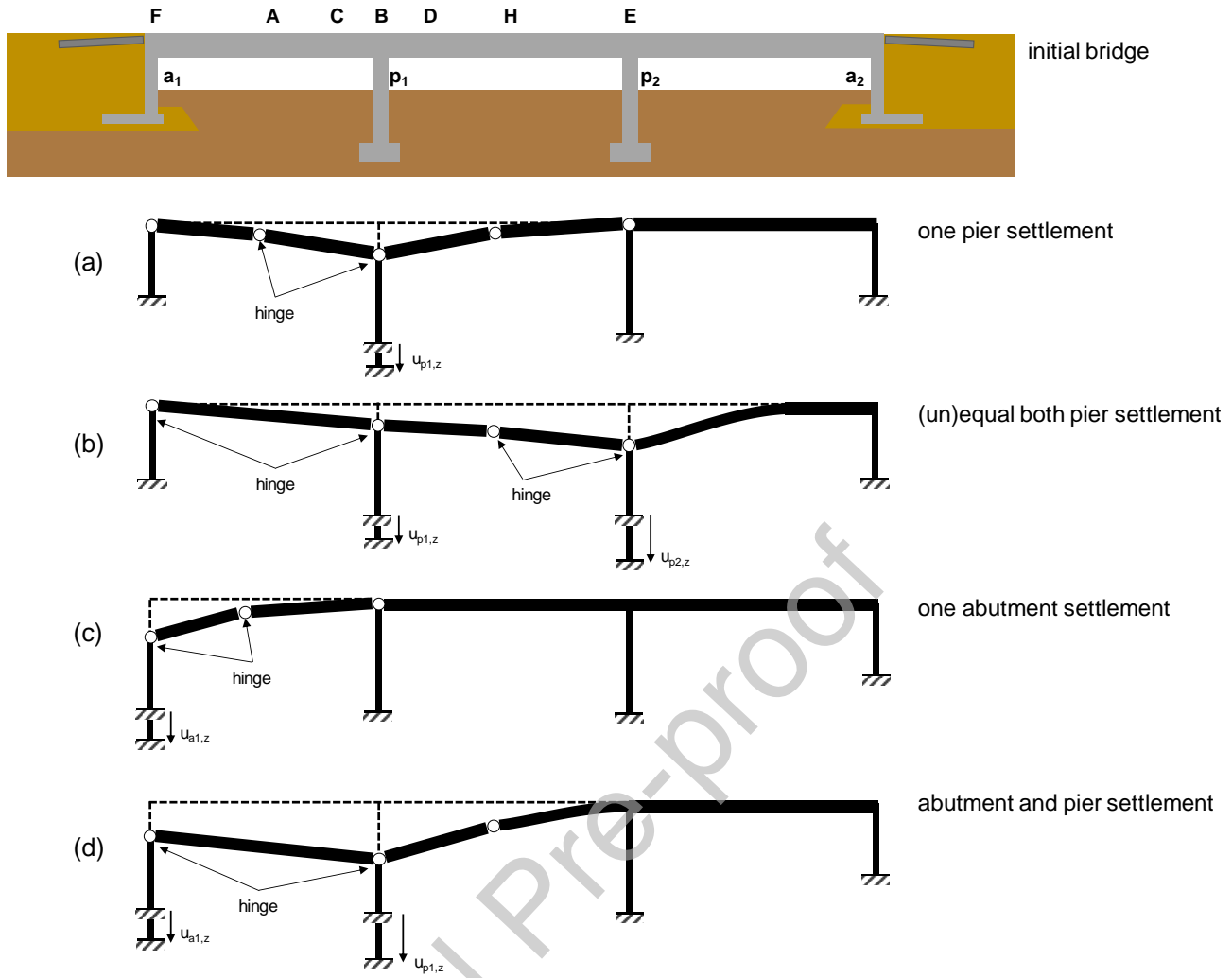


Figure 2. Sketches of potential failure mechanisms for scour-induced damage of bridges with continuous deck and/or integral piers (p) and abutments (a).

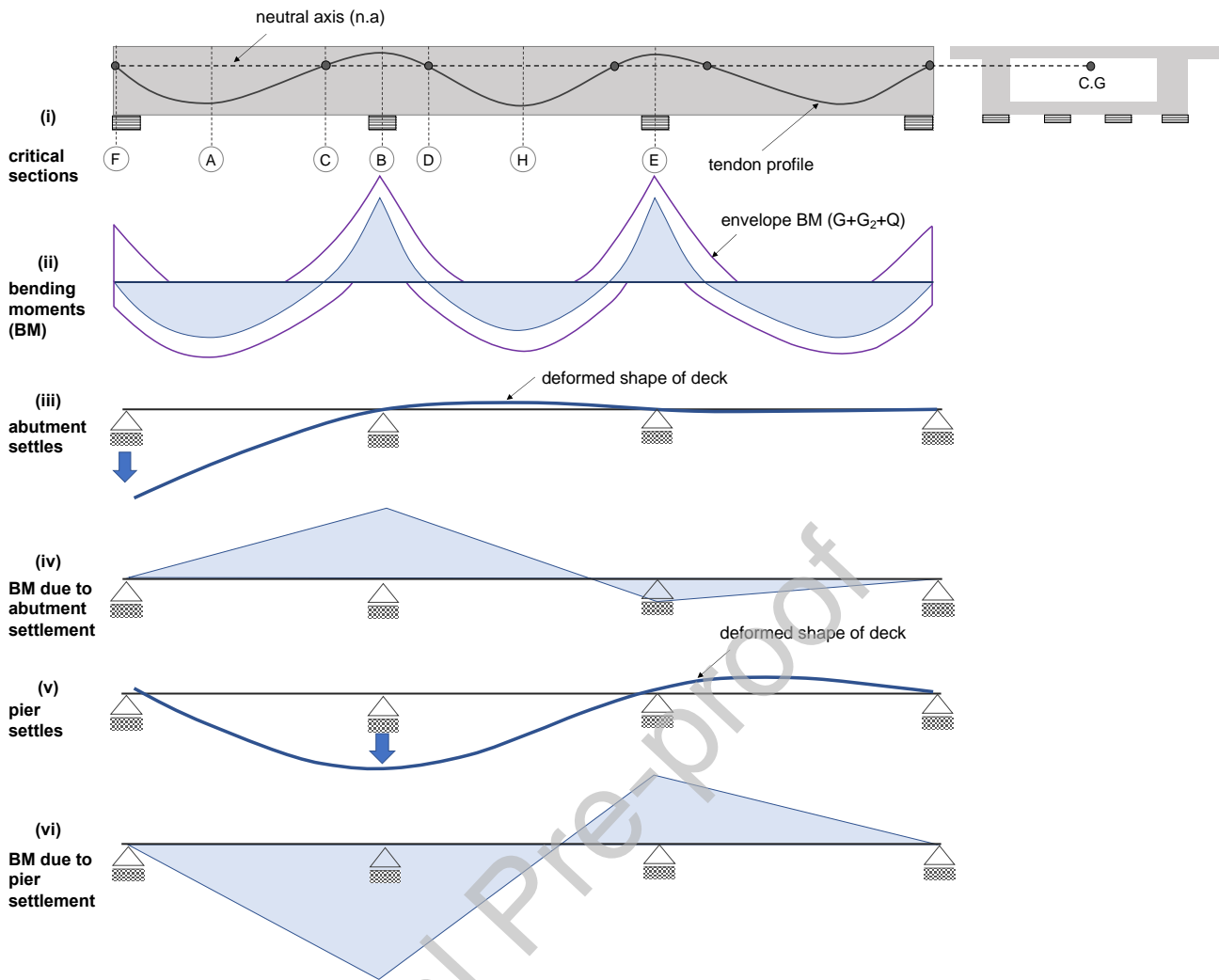


Figure 3. Critical sections (F to E) along a continuous box girder deck, tendon profile (i), envelope of bending moment (BM) diagrams for vertical loads (ii), deformed deck due to abutment scour induced settlement (iii), and corresponding BM diagram (iv), deformed deck due to pier scour induced settlement (v), and corresponding BM diagram (vi).

Figure 4 shows a typical three-span isolated bridge where the deck is seated on the wall-type piers and abutments through bearings. The deck is continuous and has a constant cross-section along the entire length of the bridge. Each of the four supports has four elastomeric bearings, which are the most common type of bearings. The geometrical and structural details of this bridge are given in Section 5. This figure illustrates the case where the shallow foundation of the pier (p1) is scoured, and this is the only structural component that is hit by the river flow. The rest of the structural components are indirectly affected by the movement of p1. The same pier receives the hydraulic forces and potential debris accumulation, as shown in the lower left of Figure 4. The rotation and movement of the top of the pier in the direction of the river upstream due to the scour hole formation, which causes part of the foundation to be vertically unsupported, results in the following: (i) the pier (p1) settles vertically downwards ($u_{p1,z}$) and simultaneously rotates in the direction of the flow upstream ($\theta_{p1,x}$). (ii) the bearings of p1 are being either under tension ($F_{p1,1}$, $F_{p1,2}$), where the rotation of the foundation leads to the downward movement of the pier, while the other two bearings (downstream) receive additional compression ($F_{p1,3}$, $F_{p1,4}$), as shown in the lower middle part of Figure 4. The tendency of the pier to move upstream can cause shearing of its bearings. (iii) The deck wants to follow the movement of the pier and rotate ($\theta_{d,x}$), however, its support on the two abutments (a1, a2) and the pier (p2), partially restricts this movement. As a result, the axial forces of the bearings on the other supports have the opposite signs to those on the

settling pier, i.e. the bearings upstream receive additional compression and the bearings downstream receive additional tension. At the same time, the net downward settlement of the pier leads to a change in the deck stresses, which can cause critical sections along the bridge deck to crack or be damaged. These positions are shown in Figure 4 (F to E) and explained in the table above. If the deck is non-continuous and includes precast I-beams and a continuity slab, the net settlement of the pier can cause extensive cracking and damage to the slab above the support, as shown in Figure 4, bottom right.

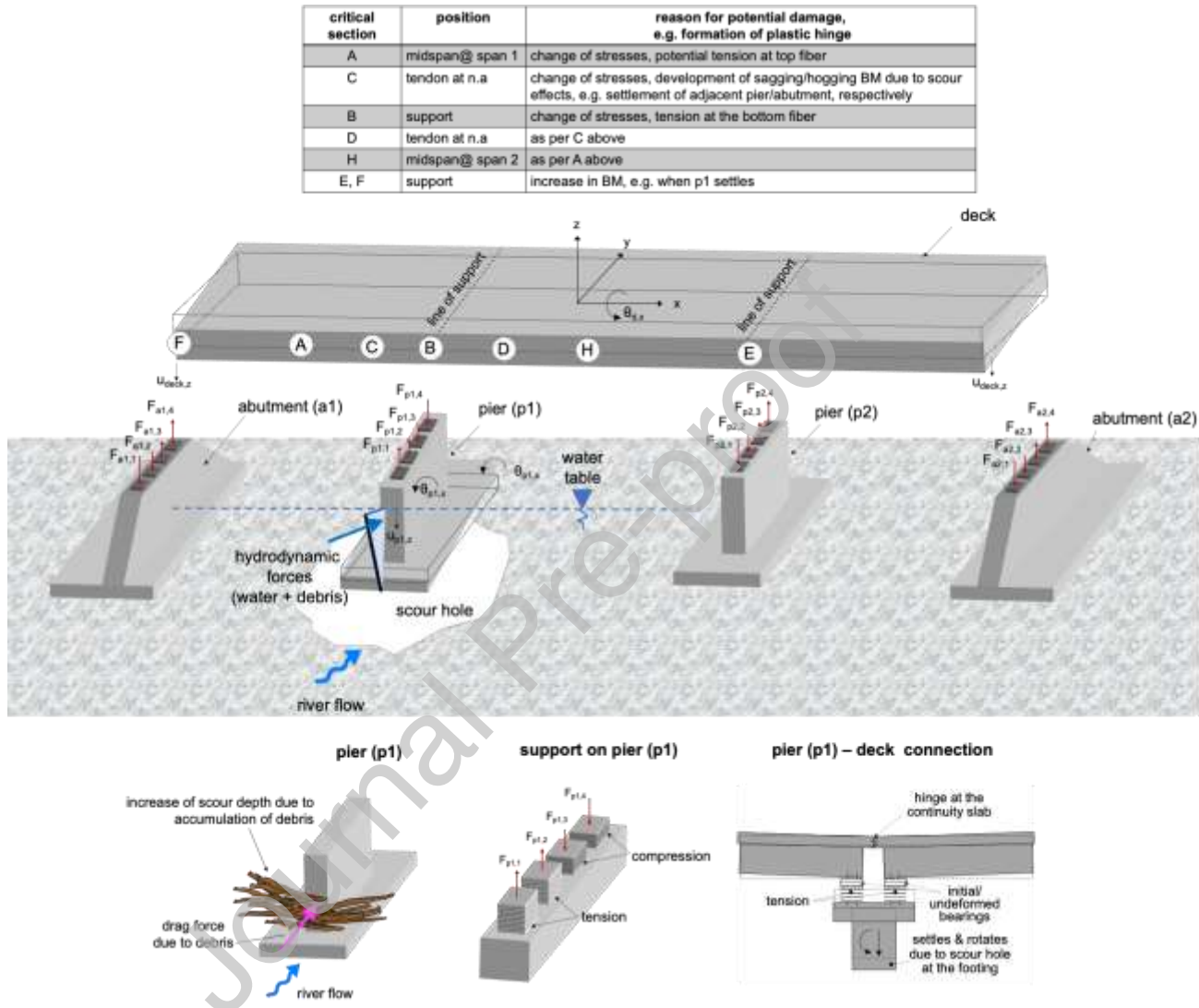


Figure 4. Interactions between bridge components, i.e. deck, bearing, piers, abutments, foundations, for pier movement due to upstream scour (indicative) and drag forces. The critical sections along the deck are also shown for a bridge with bearings.

4. Numerical modelling for fragility analysis

The generation of fragility functions based on the framework of section 2 relies on detailed numerical modelling of a three-span reinforced concrete bridge-backfills-foundation-soil system, subjected to sequences of hazards, i.e., flood, scour and earthquake. A three-dimensional (3D) numerical model is considered as the reference model for the flood and scour effects on the bridge; however, due to the extensive computation time required for conducting time-history analyses in the 3D Plaxis model, a 2D numerical model was employed for the earthquake loading, to facilitate the analyses. In this model, the earthquake excitation is applied in the longitudinal direction of the bridge. The analyses of the bridge system are performed using the finite element

code Plaxis 3D/2D v. 2019. Sectional analysis was employed to calculate the capacities of the bridge critical sections, to evaluate the damage level of the bridge.

4.1 FEM simulations

Description of the numerical model

An idealised three-span prestressed concrete bridge on shallow foundations was considered, with a total length of 100.5 m, and spans of equal lengths of 33.5 m, supported by two intermediate piers and two abutments. This is a benchmark used and validated before (Mitoulis 2020). Two types of connection between the continuous deck and the piers and abutments are examined, i.e., monolithic/fully integral connection and through bearings. The deck is a box girder with a constant cross-section along its entire length and a width of 13.5 m. The height of the abutments is 8 m, the footing has a thickness of 1m and is 5.5 m long. The piers are wall-type, with a transverse width of 4.5 m and a height of 10 m, including the 1m thick foundation footing. The longitudinal dimension of the pier is 1 m. Their shallow foundations have dimensions of 3.5 m and 6.0 m in the longitudinal and transverse direction, respectively (Figure 5) and the foundation depth (D_f) is 2.5 m. A quasi-permanent vertical load included the deck self-weight and 30% of the variable loads as per Eurocode 1 (EN1991-1-6, 2005), which was estimated at 5.5 kN/m² and was applied as an area UDL (uniformly distributed load) on the deck. The deck is prestressed with continuous tendons throughout the deck. Adequate cover was provided for the tendons at the extreme positions, i.e. upper and lower fibre of the deck. Two different prestressing forces were considered, which were -40.60 MN and -54.06 MN for the integral and the isolated bridge, correspondingly. This led to different capacities, which are reported in section 4.2 below. The passive reinforcement class is B500s, and the prestressing tendon grade is St1570/1770.

The bridge components were modelled using C30/37 concrete with a unit weight of $\gamma = 25$ kN/m³ and modulus of elasticity $E = 33 \cdot 10^6$ kN/m². The deck was modelled with plate elements in both 2D and 3D models, the piers and abutments were modelled with plate elements in the 3D model, and with cluster elements in the 2D model, while cluster elements were used to simulate the footings in both models. The hollow box girder was modelled with an equivalent plate of vertical depth 1.91m. The latter was calculated on the basis of the vertical stiffness of the real deck and second moment of area I , which was equal 2.74 m⁴, thus considering a transverse dimension of the transformed rectangular section equal to 13.5 m, $d = \sqrt{12 \cdot I / A}$, where A is the area of the real cross-section equal to 8.96 m², and a unit weight of 8.67 kN/m³. The analyses took into account the effective stiffness of the cracked structural components, i.e. EI_{eff} , and hence, they were considered to respond in a linear and elastic manner.

The monolithic connections between the deck and supports were simulated with rigid connections in the 3D model and with rotation fixities in the 2D FEM. For the isolated bridge, the selection of bearings was based on the requirement that the maximum compressive stress will not exceed 4 MPa, which led to four bearings with dimensions 800x800x100 mm per support, i.e. 16 bearings in total. The bearings were modelled with cluster elements, using linear elastic non-porous material, along with a linear elastic vertical beam at the centre of the bearing with special interface connections, simulating pinned ends. This approach enabled the modelling of elastomeric bearings whose stiffness and deformability is anisotropic, i.e. direction-dependent. Elastomeric bearings have relatively low stiffness for horizontal movements, parallel to the steel reinforcements and this is equal to the shear stiffness, which is dependent on the shear modulus G , the shear area of the isolator A , and the total thickness of the elastomer $\sum t_i$, where t_i is the thickness of each elastomeric layer. Vertically, the isolators are substantially stiffer as they are expected to underpin the deck, additional permanent and traffic loads (see Mitoulis, 2015). In addition, elastomeric bearings provide allowance for small rotations, yet, they are insignificant in comparison with their shear displacements, and therefore no damage states were related to these rotations. To model the above direction-dependent behaviour in Plaxis, a cluster element with a shear

modulus $G=1000 \text{ kN/m}^2$, modulus of elasticity $E=2980 \text{ kN/m}^2$, unit weight $\gamma=29 \text{ kN/m}^3$ was used. At the same time, the stiff vertical beam, which was deployed along the vertical axis of the elastomeric bearings with Young's modulus $E_b=125 \cdot 10^3 \text{ kN/m}^2$. The latter value was calculated on the basis of closed-form solutions provided by Kelly and Konstantinidis (2011) and results in a small (3 mm) vertical displacements under the deck quasi-permanent loads. The allowance for rotations was provided through the interface properties, i.e. fixed translation and free rotation. The bearings sit on structural plates with negligible unit weight and equivalent properties to the piers/abutments. Further information on the modelling and the properties of the bridge can be found in Mitoulis (2020).

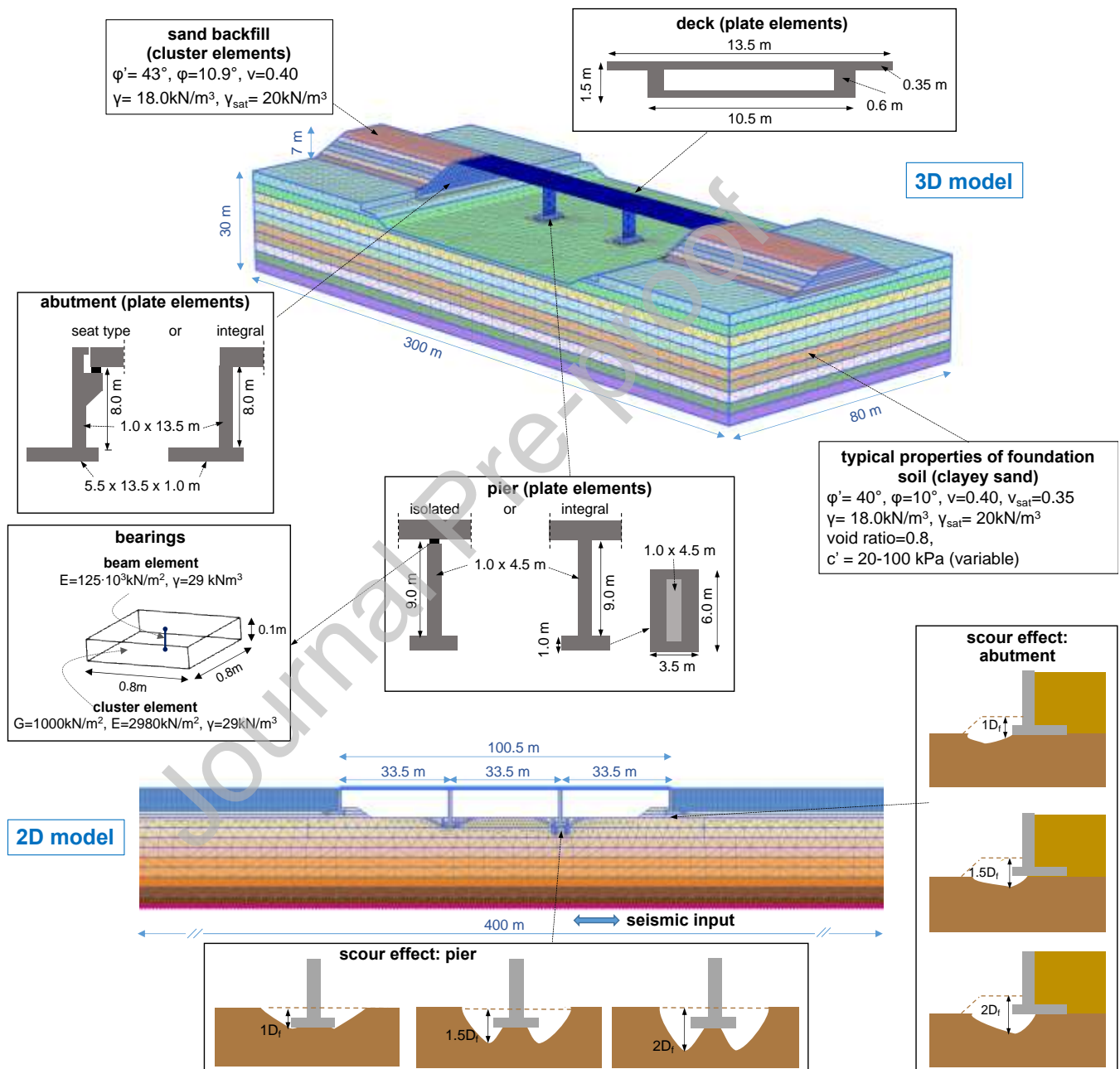


Figure 5. 3D and 2D FEM model of the bridge, backfill and foundation soil, and details of the bridge. Indicative scour hole formations are illustrated for the 2D model.

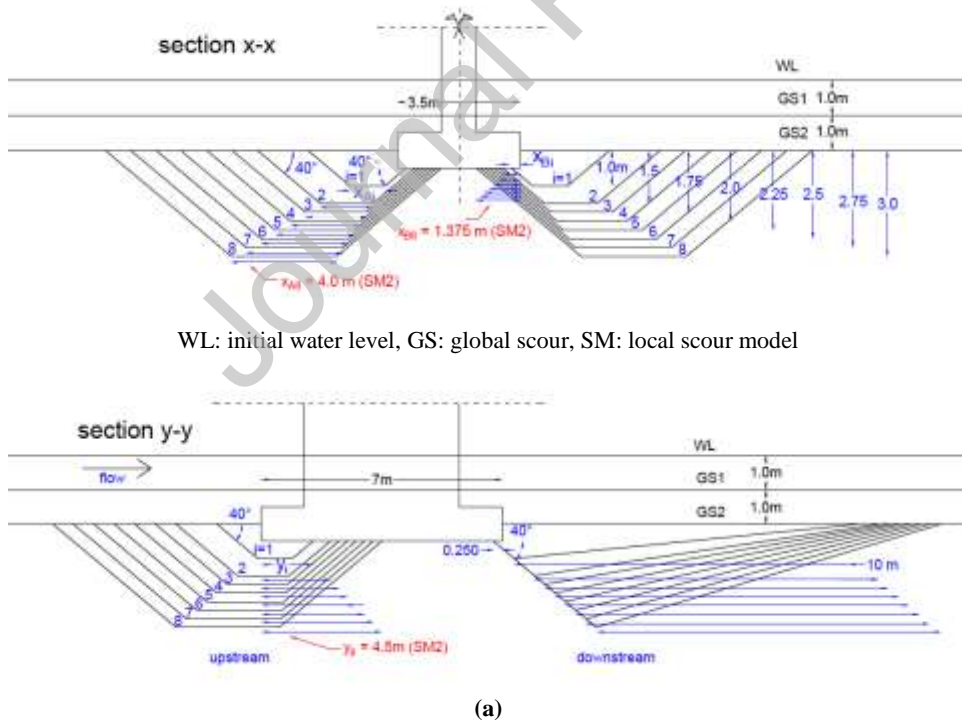
The foundation soil is a clayey sand classified as ground type C according to Eurocode 8 (EN 1998-1, 2004). The unsaturated and saturated unit weight is $\gamma = 18 \text{ kN/m}^3$ and $\gamma_{\text{sat}} = 20 \text{ kN/m}^3$, with a Poisson's ratio $\nu = 0.40$ for unsaturated and 0.35 for saturated conditions, angle of friction $\phi' = 40^\circ$ and dilation $\phi = 10^\circ$. The variation of the maximum shear modulus with depth was defined according to Hardin (1978) for sand material. The first 3 m of soil at the free end of the abutment and pier excavations are sloped. The backfill has a 1:2 slope and it consists of well-compacted sand with $\phi' = 43^\circ$ and $\gamma = 18 \text{ kN/m}^3$. For all the analysis phases, an elastoplastic soil behaviour, i.e. Mohr-Coulomb criterion is assumed. To model the interface between the abutment and the backfill, and the footings and the foundation soil, interface elements with a friction coefficient of $R_{\text{inter}} = 0.8$ were used. A calibration procedure is followed to account for the dependency of stiffness and damping on the primary shear strain level during the earthquake (Argyroudis and Kaynia 2015). To minimise the boundary effects on the structure adequate model length and width was employed in both models following a sensitivity analysis (Figure 5). All analyses included initial stages to simulate the initial geostatic stresses and the construction of the bridge, i.e. excavation, construction of footings, piers, abutments, backfills, deck and imposed load. The Plaxis normally fixed and fully fixed conditions were selected for the lateral and lower boundaries, respectively, for both the 2D and 3D models, whilst, the tied degrees of freedom were assigned for the lateral boundaries during the dynamic phase in the 2D model.

Flood effects: scour, hydraulic forces and debris

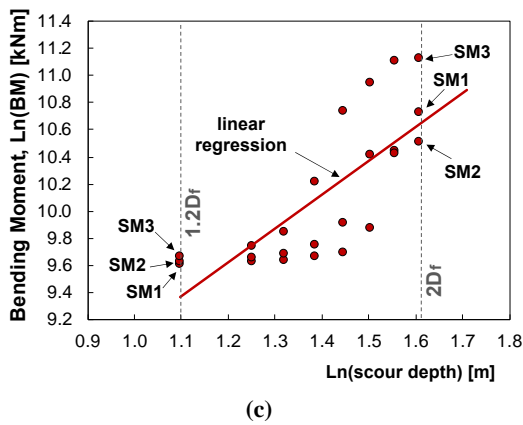
The formation of the scour hole, including the depth and its extension in relation to the dimensions of the foundation that is being affected, depends on the type of foundation, the characteristics of the flow, the soil type and its conditions, and the riverbed. As a result, the formation of the scour hole and its geometry is a very random and highly uncertain event (Briaud, 2015). Uncertainties in flood depth and flood duration are also critical (Nofal et al. 2020). A common practice is to consider identical scour depths at all bridge piers corresponding to flood events of specific return periods (e.g. Banerjee and Prasad 2013; Guo et al., 2016) or to analyse a range of scour depths. More recently, Yilmaz et al. (2016) assumed a variation of scour depths across multiple piers, based on streamflow statistics and regional regression equations, while Tubaldi et al. (2017) proposed a probabilistic framework to estimate the temporal evolution of the scour depth by combining hydrological data and scour analysis. Other studies have assumed deterministic scour depths based on closed-form solutions or experiments (e.g. Arneson et al., 2012; Pizarro et al. 2017, 2020), yet, this approach could lead to overly conservative scour estimates. The uncertainty of scour risk and its time dependence is rarely considered (Guo et al., 2016). Briaud et al. (2014) concluded after a systematic statistical analysis of a large number of measured pier scour depth databases, that the calculated scour depths may on average exceed full-scale measurements by a factor of about 3, a proof of the high uncertainty of scour models.

In the context of this work, engineering judgement was used, whereby a variable scour hole depth of one to two foundation depths ($1-2D_f$) was considered, with a step of $0.1D_f$, while different scour hole geometries were formed and analysed. These scour depths correspond to water discharges (Q) and flow depths (y_o) on the basis the HEC-18 equation considering typical channel width, $B=75 \text{ m}$, river-bed slope $S_o=0.002 \text{ m/m}$ and Manning of the channel bed, $n=0.06 \text{ m}^{-1/3}\text{s}$. It is assumed that the initial water table is at the lower boundary of the model, which corresponds to dry soil conditions, while it is gradually raised to 3 m above the soil surface, to simulate flooding conditions, in this case taking into account the saturated state of the soil. It was assumed that the scour effects begin when this water level is reached. The global scour (GS) is initially carried out in two steps, by removing 1 m of the riverbed in each step, GS1 and GS2. Subsequently, local scour effect is modelled by introducing discrete phases by increasing the scour depth with a step of $0.1D_f$ and removing soil clusters around the foundation to simulate gradual sediment removal. Therefore, the formation of the scour hole was based on a gradual removal of the soil and it was not a result of numerical analysis.

The **flooding effects** were modelled taking into account the formation and uncertainty in the geometry of the scour hole, hydraulic forces and the accumulation of debris on the piers (Panici and de Almeida 2020). The latter causes a further restriction of the flow and by increasing the effective area of the supports, which in turn increases the drag force and the scour depth, according to Arneson et al. (2012). The drag force and the increased scour depths were calculated with back analysis, for an initial (without debris) scour depth ranging from 0 to $2D_f$. More specifically, the discharge was considered in the range of 20 to 1500 m^3/s , and this resulted in flow depths y_0 of about 0.50 to 7.0 m, thus affecting the piers but not the deck. The total drag force is the result of the water and the debris accumulation according to Eurocode 1 (EN 1991-1-6, 2005). The resulting drag force due to water acting on the pier was between 0.60 and 70 kN and on the debris, was between 0.4 and 47 kN, assuming a triangular shape of the debris accumulation with a width of 4 m (longitudinal to the bridge) and a depth equal to half of y_0+2m , where the 2 m correspond to the depth of GS. The total drag force was very low and hence, unlikely to significantly affect the global behaviour of the bridge. Taking into account the effective pier width, and correction factors for the square pier nose, the flow perpendicular to the pier and the clear-water scour bed condition, an increase in scour depth up to about 20% was estimated based on Arneson et al. (2012), whereas a debris width of 24 m would double the scour depth, i.e. up to 6.7 m. The increase of the debris width from 4 to 24 m would cause an increase of the drag force to 155 kN, also reported in Panici and de Almeida (2018), which would have a minor impact on the response of the pier. Based on Huang and Xiao (2009) the drag force becomes important when the water overtops the deck. However, the increase of the scour depth for this debris width, based on the numerical results exceeds by far the threshold for bridge collapse. The latter is based on a sensitivity analysis, which showed that the system fails for scour depths larger than $2.0D_f$, i.e. 5 m, an indication of the vulnerability of bridges with spread foundations. Hence, considering larger debris widths for this system does not provide any further insights.



	SM1	SM2	SM3
x_{A1}	1.00	2.00	3.00
x_{A2}	1.50	2.50	3.50
x_{A3}	1.75	2.75	3.75
x_{A4}	2.00	3.00	4.00
x_{A5}	2.25	3.25	4.25
x_{A6}	2.50	3.50	4.50
x_{A7}	2.75	3.75	4.75
x_{A8}	3.00	4.00	5.00
x_{B1}	0.250	0.375	0.500
x_{B2}	0.500	0.625	0.750
x_{B3}	0.625	0.750	0.875
x_{B4}	0.750	0.875	1.000
x_{B5}	0.875	1.000	1.125
x_{B6}	1.000	1.125	1.250
x_{B7}	1.125	1.250	1.375
x_{B8}	1.250	1.375	1.500
y_1	1.50	2.50	3.50
y_2	2.00	3.00	4.00
y_3	2.25	3.25	4.25
y_4	2.50	3.50	4.50
y_5	2.75	3.75	4.75
y_6	3.00	4.00	5.00
y_7	3.25	4.25	5.25
y_8	3.50	4.50	5.50



(c)

component	β_D	
	one pier scoured	two piers scoured
integral bridge		
deck section F/A/B/H/E	0.41/0.23/0.88/0.26/0.30	0.48/-/0.86/0.46/0.90
abutment (a1, a2)	0.41	0.49
bridge with bearings		
deck section A/B/H/E	0.39/0.38/0.38/0.37	0.63/0.35/1.06/0.48
pier (p1)	0.89	1.25

(d)

Figure 6. (a) Scour models (SM_i) with variable geometries: longitudinal section with symmetric scour geometry (top) and transverse section at the pier with non-symmetric scour hole geometries upstream and downstream (bottom).

(b) Dimensions x_{Li} , x_{Ri} , y_i are provided for each SM. (c) Example of variation of the calculated EDP (BM) on deck section F of the integral bridge, when different scour models (SM) shown in (a) and (b), are employed in the numerical model. (d) Indicative β_D values for different bridge components.

With regard to the **location of the scour hole**, the 2D model considered either scour formation at one pier or one abutment. The pier scour took into account the randomness of soil erosion, which is why two different cases were considered (Zampieri et al., 2017). In the first case, a one-sided scouring was considered, whereas in the second case scour occurs on both sides of the pier in the framework of a sensitivity analysis. It should be noted that the scour formation in the longitudinal direction of the bridge was simulated considering different geometries, while in the transverse direction it was assumed that this scour hole extends over the entire width of the foundation. However, the 2D model is not capable of taking into account the transverse hydraulic forces or the accumulation of debris. In the same model, the scour effect was analysed either for a single pier or an abutment or for both piers. In an effort to more accurately simulate the combination of different hydraulic stressors, namely, scour hole, hydraulic forces and debris accumulation, a 3D model was also built in Plaxis. The model took into account the formation of scour holes at the foundation of one or two piers and at the foundation of the abutment. The latter had only a very small influence on the deformation of the bridge, as the settlements of the abutment were negligible. The reason for this was that the abutment was founded over an extensive foundation, including the foundation of the wing walls and as a result soil settlements were minimum. Figure 6 shows the different scour hole geometries analysed with variable dimensions upstream and downstream. The slope of the scour hole was considered to be 40° , i.e. equal to the angle of friction of the foundation soil.

Multihazard actions

In this section hazard actions are described for sequences of flood induced scour and earthquake excitations. The analysis at the initiation of the earthquake excitation took into account the existing damage of the bridge on the basis of altered boundary conditions due to scour hole formation, plasticity in the soil, settlement of the foundation, accumulation of deflections in the bridge, and redistribution of actions in the structural components.

Acceleration time histories recorded on rock or very stiff soil were selected as outcrop motion for the analyses of the 2D model on the basis of spectral matching (Jayaram et al. 2011). The minimum number of five ground motions for dynamic analysis were employed (EN 1998-1), including the following records (see Mitoulis 2020): Kocaeli (Gebze), Turkey, 1999, 7.6 M_w ; Parnitha (Kypseli), Greece, 1999, 6.0 M_w ; Duzce (Ldeo Station No. C1058 Bv), Turkey, 1999, 7.2 M_w ; Umbria Marche (Gubbio-Piana), Italy, 1998, 5.0 M_w ; Hector

Mine, USA, 1999, 7.1 M_w . The time histories were scaled to PGAs of 0.2, 0.4 and 0.6g and applied separately for each scour depth, i.e. $0D_f$, $1D_f$, $1.5D_f$, $2D_f$, simulating the sequential occurrence of the two hazards. Therefore, a total of 60 combinations were analysed for each bridge type and scour condition, i.e. 4 scour levels, 5 inputs, 3 PGA levels.

Definition of damage states

The maximum bending moment (M_{max}) is selected as the EDP for the critical sections of the deck, pier and abutment as representative of the structural failure. Cracking of the concrete and yielding of the steel are selected as the thresholds for the minor damage state of the bridge deck and pier/abutment, respectively (Table 2, columns 1, 2). The yielding bending moment (M_y) defines the moderate damage for the deck, while the thresholds for the extensive and complete damage state of the deck correspond to $1.5M_y$ and $2M_y$, respectively. These assumptions are based on engineering judgement, the literature (Tsionis and Fardis 2014) and the empirical equal displacement rule (Aydinoglu 2004). For the pier and abutment, the corresponding thresholds are $1.5M_y$, $2.0M_y$ and $2.5M_y$. Five critical sections of the deck, i.e. sections F to E in Figure 3, were identified and their moment-curvature curves were calculated through section analysis to define the cracking and yielding moments. Also, the drift ratio is considered as an alternative EDP for the pier and abutment, and the damage thresholds defined by Kim and Shinozuka (2004) were adopted (Table 2, column 3). The thresholds for the bearings limit states have defined based on Mitoulis (2015). The maximum permanent ground deformation of the backfill behind the abutment and the soil under the foundations is defined as the EDP for the geotechnical failure. The thresholds for the backfill damage described by Argyroudis et al. (2015) are adopted (Table 2, column 6) and the thresholds of column 5 in Table 2 are considered for the foundation (as per Mitoulis et al. 2020).

Table 2. Damage state definitions for bridge components.

component	deck (1)	pier/abutment (2)	pier/abutment (3)	bearings (4)	foundation (5)	backfill (6)
engineering demand parameter (EDP)	BM	BM	drift ratio [%]	displacements: shear/compressive/tensile [mm]	settlement [m]	settlement [m]
damage type:	STR	STR	STR	STR	GEO	GEO
damage state						
minor	M_{cr}	M_y	0.70	10/5/2.5	0.015	0.05
moderate	M_y	$1.5M_y$	1.50	20/10/5	0.035	0.15
extensive	$1.5M_y$	$2.0M_y$	2.50	50/15/10	0.090	0.40
complete	$2.0M_y$	$2.5M_y$	5.00	100/20/20	0.140	0.40

BM: bending moment; M_{cr} : cracking BM; M_y : yielding BM (M_{cr} and M_y are different for each critical section F to E)

4.2 Results and discussion on FEM analyses

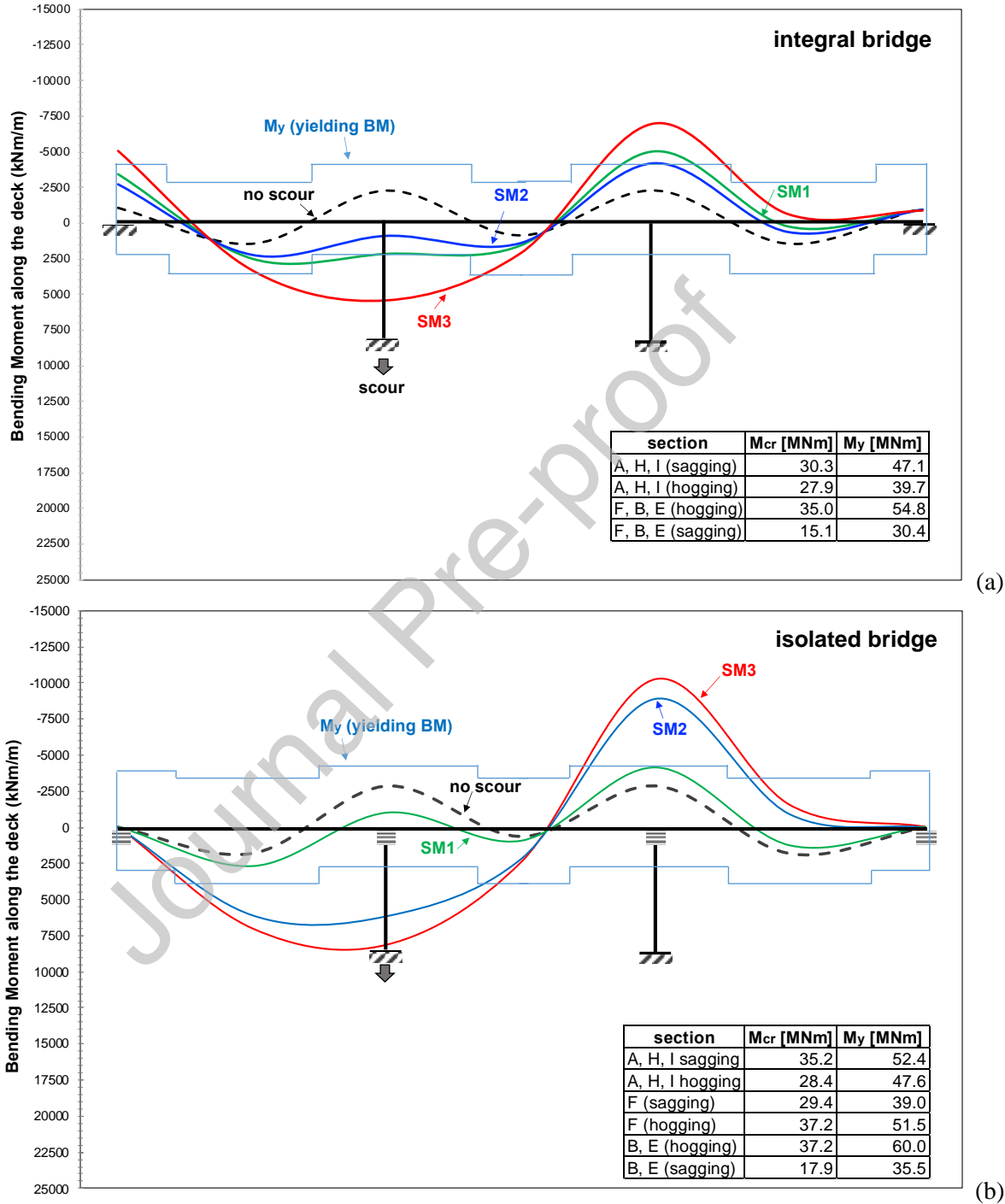
Response of 3D model for flood effects

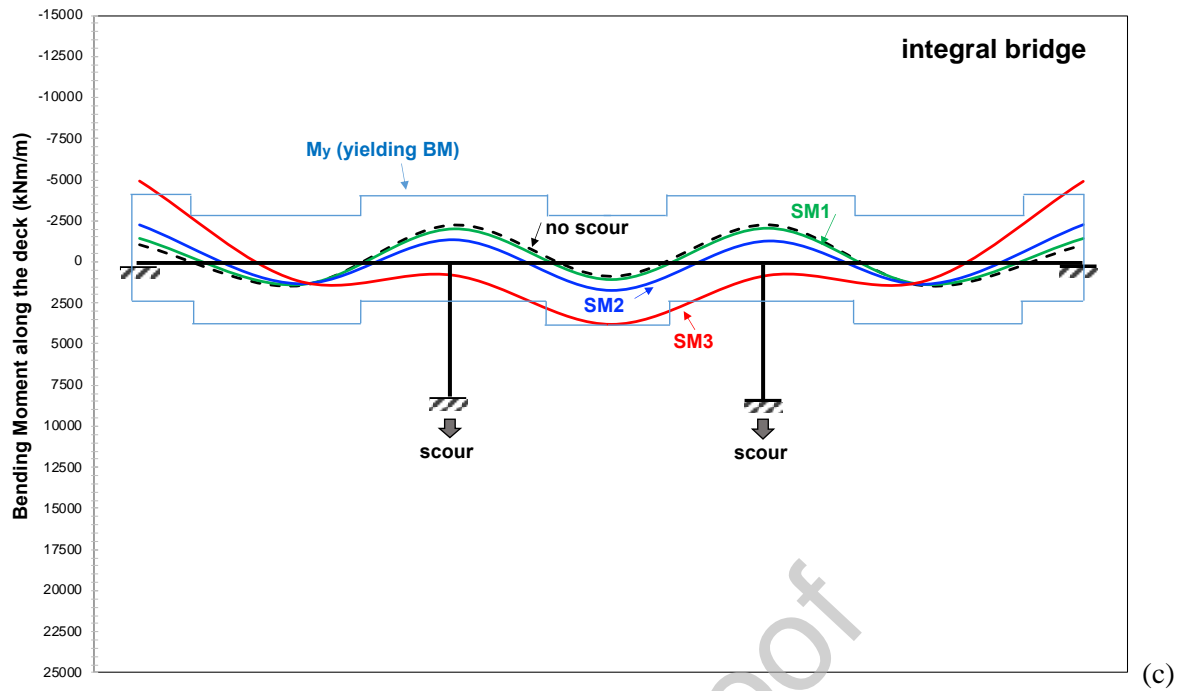
Figures 7a to 7d show the envelopes of the bending moment (BM) diagrams for the deck for different bridge types, variable scour models (SM) at maximum scour depth, and considering different positions of the local scour, i.e. scour at one or both piers. The BM shown here are per unit length of the bridge width, and therefore, the total BM can be calculated by multiplying the values shown in the diagrams by the bridge width, i.e. 13.5 m. The figure shows the evolution of the BM compared to the original state, i.e. without scour (dashed black line), and the corresponding BM for the maximum scour depth for each SM. Of the three SMs, SM3, based on Figure 6 is the most severe, while SM1 is the least critical. This explains why BMs drastically change from SM1 to SM2 and ultimately to SM3. Together with the actions (BM), the bending capacities (M_y) of the deck are also given, as calculated by sectional analysis, taking into account the passive reinforcements and prestressing steel of the deck. The latter evaluated the maximum sagging and the hogging of BMs at all supports and mid-spans.

In all cases, it appears that the BM above the scoured pier is reduced due to the settlement and the hogging BM is transferred to the adjacent support. At the same time, the sagging BM of the first span is increased, while the third span suffers from the inversion of the BM sign to a hogging BM. This mainly affects the isolated bridge, whilst the integral bridge suffers less from the scoured foundation, as the pier, which is rigidly connected to the deck, does not settle uncontrollably, but is been assisted by the adjacent supports. As a result, the integral bridge does not experience any dramatic change in its BMs, compared to its isolated counterpart.

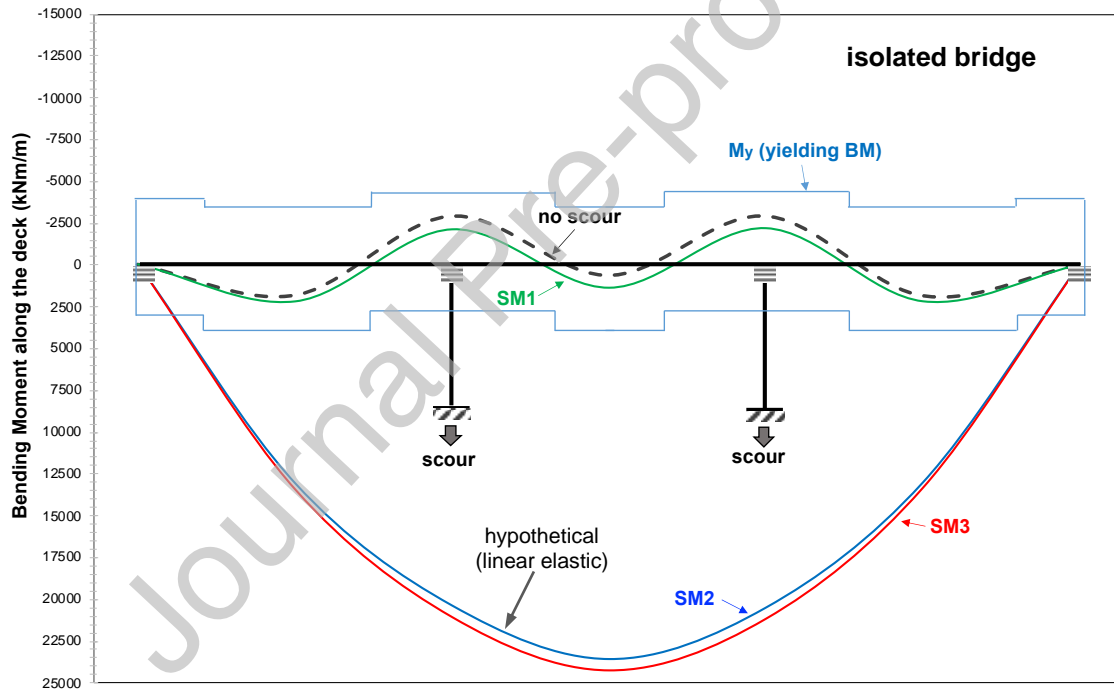
Looking at the second set of plots, which relate to the case where both piers are scoured, it can be seen that the integral bridge successfully copes with the stressor of global settlement, as the BMs change significantly, but do not seem to exceed the capacities substantially. On the contrary, the isolated bridge seems to lose its two intermediate supports when SM2 or SM3 are considered. The deck as a result responds as a simply supported beam, which far exceeds its flexural capacities (Fig. 7d). It should be noted that in reality the deck would never reach the BMs shown in Fig. 7d because it will yield when the BMs reach the value of approximately 52.4 MNm or 3.88 MNm/m for the 13.5 m transverse dimension of the deck. In these figures, the cracking BM (M_{cr}) and the yielding BM (M_y) are given in MNm. The M_{cr} is calculated on the basis of the simple beam theory $M_{cr} = \sigma I / y$, where σ is the sum of f_{ctm} and σ_{cp} , I is the second moment of area of the deck (2.74 m^4) and y is the distance of the centre of gravity of the deck from the upper fibre (0.66 m) or the lower fibre (0.83 m). The f_{ctm} (EN 1992-1-1, 2004) is 2.9 MPa, and σ_{cp} is the compressive stress due to the prestressing force, e.g. $54.06/8.96 = 6.03 \text{ MPa}$ for the isolated bridge and 8.96 m^2 is the area of the deck. It should be noted that M_{cr} fluctuates when the axial load in the deck changes.

Figure 8 shows the settlement of the pier when one or both piers are scoured, for the integral (blue lines) and isolated (red lines) bridge, in the case of SM2. From the figure it can be extracted that the integral bridge copes with smaller settlements when a single pier is scoured, whereas the severity of both types of bridge is similar when both piers are scoured. However, it appears that the isolated bridge has relatively smaller settlements at the same extreme scour depth of greater than $1.7D_f$.



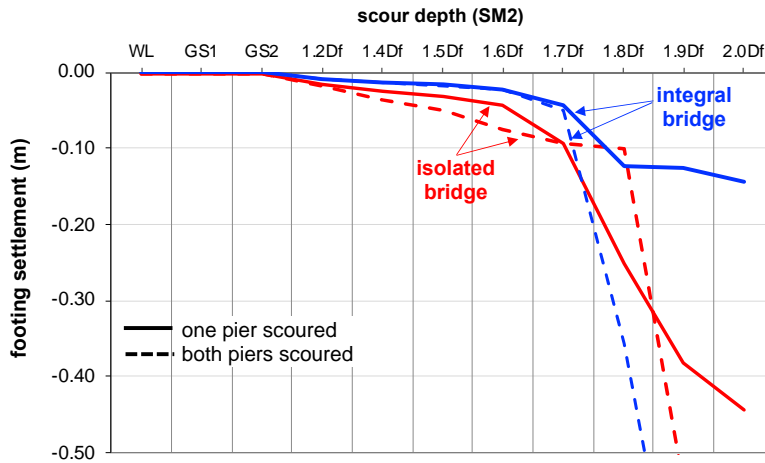


(c)

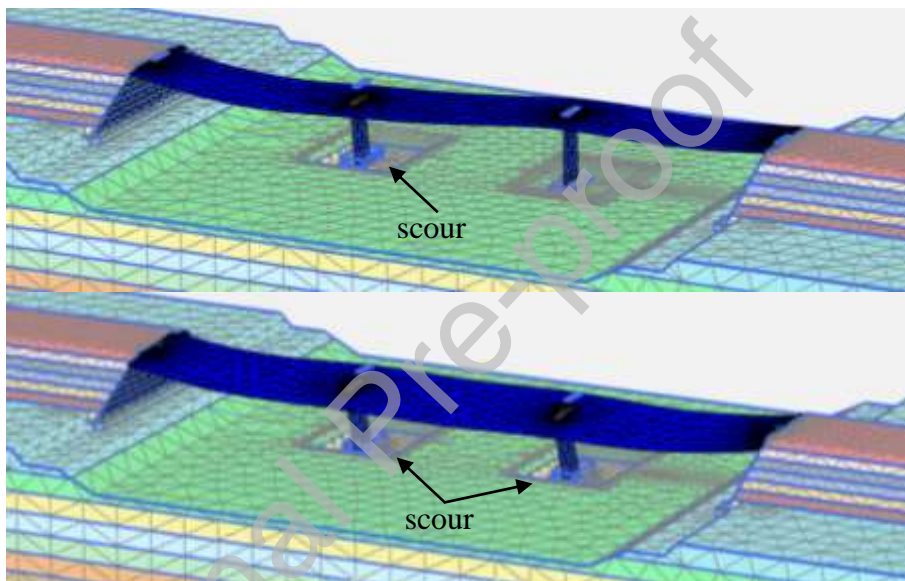


(d)

Figure 7. Bending moments (BM) along the deck per unit width of the integral and isolated bridge for the maximum scour depth of three local scour models (SM1, SM2, SM3 as per Figures 6a and 6b). Left pier scour (a and b) and both piers scour (c and d). The BM in the tables have to be divided by 13.5 m to obtain the BM along the M_y of the diagram.



(a)



(b)

Figure 8. (a) Pier footing settlements for the integral and isolated bridge, for one and both piers scouring, as per SM2 (settlements are excessive for scour depths above $1.9D_f$), (b) Deformed bridge for one and both piers scouring.

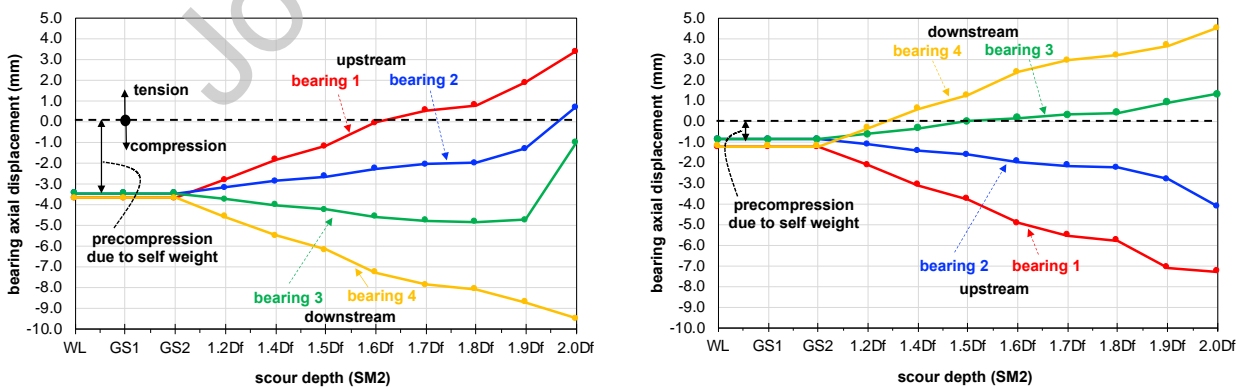


Figure 9. Axial displacements of bearings when both piers are scoured to SM2. Bearings on the pier (left) and on the abutment (right) are shown, where 1 is the first bearing upstream and 4 is the last bearing downstream.

Figure 9 shows the evolution of the axial displacements of the bearings from the initiation of global scouring to the formation of $2.0D_f$ local scouring. Both figures refer to SM2, whilst the left figure shows the results for

the pier bearings and the right figure shows the results for the abutment bearings. As described in Figure 4 for one pier, the formation of the scour hole in both piers similarly intensifies the upstream rotations of the piers. As a result, and assuming that the deck is supported by the abutments, bearings 1 and 2 on the piers will be under tension as the pier cap moves away from the lower fibre of the deck. At the same time, the weight of the deck has now been transferred to the remaining pier bearings (3 and 4), which receive additional compression. The deck tends to rotate in the upstream direction and follow the pier cap as it moves downwards, causing bearings 1 and 2 on the abutments to experience additional compression, whilst 3 and 4 are unloaded and under tension. More bearings can be decompressed for greater rotation of the pier, e.g. see bearing 3 in Figure 9 on the left. It should be noted that the bearings may fail under axial tension (cavitation) or overcompression (buckling) and/or shear as shown in Table 2.

Response for flood and earthquake effects

Figure 10 shows the BM diagram along the bridge deck where the pier or abutment were scoured, followed by seismic shaking based on 2D numerical simulations. The different BM diagrams correspond to either different scour depths and/or variable earthquake excitations, which are described in section 4.1. Similar behaviour was observed for flood only effects (see Figure 7), where the settlement of the scoured pier leads to the inversion of the BM sign from hogging to sagging and to the transfer of the additional BM to adjacent supports, i.e. to the pier on the left and the abutment on the right (Fig. 10a, c). When the piers are rigidly connected to the deck, they attract most of the BM, and therefore, the increase in BM within the first span was relatively small (Fig. 10a). The opposite was observed for the isolated bridge (Fig. 10c), as no BM is transferred through the bearings to the piers, resulting in a significant BM received by the first span as a result of the settlement of p2. A similar transfer of BM was observed during the settlement of the abutment (Fig. 10b).

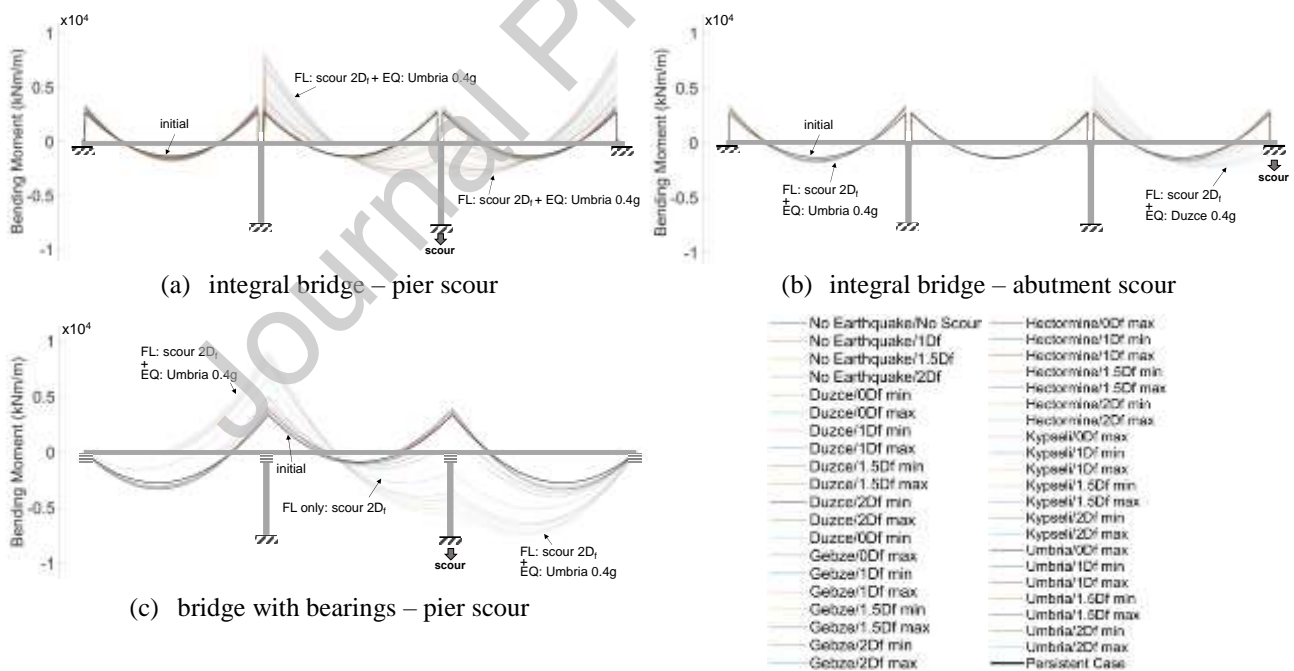


Figure 10. Envelope of bending moments (BM) per unit width along the deck, for integral bridge (a, b) and bridge with bearings (c), for different scour conditions, i.e. no scour, 1.0D_f, 1.5D_f, 2.0D_f, followed by earthquake excitations for PGA of 0.4g. Black curve shows the initial BM.

5 Fragility functions

The generation of fragility functions for each bridge component was based on the correlation of the intensity measure (IM), i.e. scour depth for floods or PGA for earthquakes, and the corresponding EDP (see Table 2). The latter was estimated based on the results of the numerical simulations, e.g. see Figure 7 for BM along the deck, taking into account different scour models and seismic hazard actions considering the uncertainty in the demand (β_D) (Fig. 6). The variation of hazard intensities and their consequences, i.e. scour hole geometry for FL and ground motions for EQ, resulted in a range of calculated EDPs, an example of which is shown in Figure 6c. A best-fit regression (Fig. 6c) was deployed to derive the median threshold intensity measure (IM_{mi}) at each damage state for all bridge components (McKenna et al. 2020), using the corresponding threshold values in Table 2. The uncertainty due to the hazard actions (β_D) is estimated based on the standard deviation of the residuals of the calculated EDPs against the best fit regression. Different β_D values are calculated for each component of the bridge, depending on the scour location (Fig. 6d). The largest scatter is observed for piers in the isolated bridge when scour is generalised. The EDP in this case is the settlement of the pier footing. The latter depends on the soil behaviour under different scour conditions (SM1, SM2, SM3), whereas the nonlinearity of the soil explains the greater variability of the observed settlements when the scour is more generalised. The total uncertainty was calculated according to Eq. 2 (see also step vi in section 2). The fragility of the system was derived from the fragilities of the components according to Eq. 3. In particular, a lower and an upper bound were estimated as per Eq. 3 on Figure 1 (bottom right). For the real system the fragility curve lies between these bounds (see also step vi in section 2).

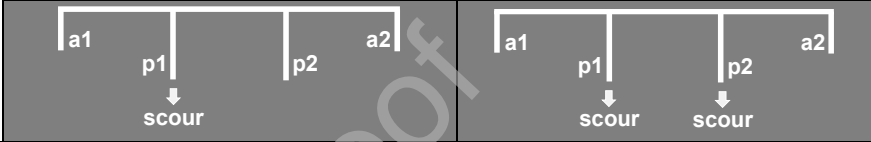
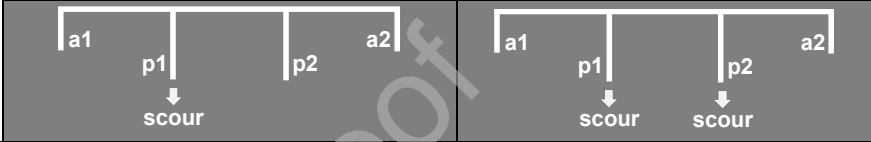
With regard to the selection of IM, the PGA was used for earthquakes as this is the most common IM in the literature (Argyroudis et al., 2019). For flood hazard, different IMs were evaluated on the basis of a sensitivity analysis, to determine the most efficient, sufficient and practicable one (i.e. scour depth, water velocity, flow depth). Based on the sensitivity analysis, it was decided that scour depth is representative of flood-induced stressors, e.g. soil erosion and debris accumulation, while in practice scour depth can be measured after the flood as opposed to other IMs that occur during flooding. Furthermore, design and assessment guidelines mainly link bridge failure to scour formation with (BD 97/12, 2012; Arneson et al. 2012). Therefore, the fragility models shown in this paper were expressed on the basis of scour depth.

Fragility functions parameters for each vulnerable bridge component exposed to flood effects can be constructed using the values of Table 3 for one and both piers scour. The abutments were not included in this table because their extensive foundation prevented scour damage. The most critical components appear to be the ones that have the smallest median values in column (3) or (5) respectively and are therefore damaged at lower IMs. An indicator for the influence of the scour geometry is the different values of standard deviation (columns 4 and 6). It is obvious that some structural components, e.g. deck section B of the integral bridge or pier 1 of the bridge with bearings, have the highest values of β_{tot} , whereas components further away from the settling pier seem to be affected less, e.g. section A or H.

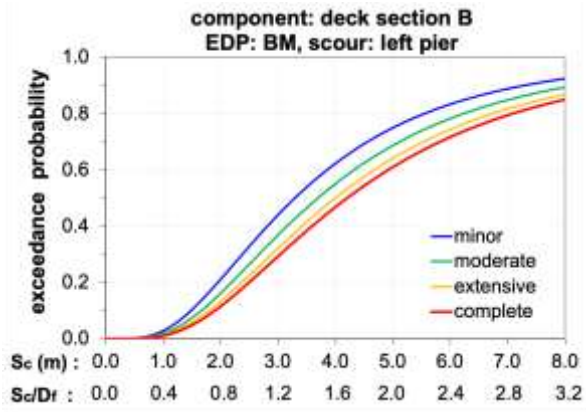
For the **box-girder deck**, the fragility curves for hogging and sagging BMs were generated, taking into account the settlements of one or both piers, due to individual or combined flood stressors, i.e. scour, debris and hydrodynamic forces. The fragility functions for the most critical deck sections are shown here, i.e. B and E in Figures 11a and 11b, and they take into account all flood-related stressors when one pier is scoured. These fragility curves apply to the isolated bridge, where the deck is seating on the piers through bearings. By comparing the two figures, it is clear that deck section E is likely to suffer minor damage in the event of minor flood stressors, yet, section B is more sensitive when it comes to extensive and complete damage. The same sections B and E are the critical sections, when both piers suffer from flood stressors. The **piers** appear to suffer similarly, regardless of whether one or two piers are affected by scour (Figures 11c and 11d). However, it seems that the piers experience the transition from minor to complete damage more quickly, when both of their foundations settle due to scouring, as indicated by the small distance between the four fragilities in Figure 11d.

Looking at the vulnerability of the **bearings**, the fragility curves for the abutments are shown, for shear and tension, whilst the high compressive capacity of the isolators has minimised the potential failures due to overcompression. Figures 11e and 11f show the fragility of the isolators under shear, for the left (a1) and the right (a2) abutment, when only the left pier (p1) is scoured. Due to the proximity of a1 to p1, the bearings on this abutment demonstrated greater vulnerabilities, compared to the bearings on a2, which showed only minor and moderate damages during extreme flood events. The bearings appear to be more vulnerable to minor damage under shear (Fig. 11e) compared to the bearings under tension (Fig. 11g), whereas the bearings of the abutment which are under tension are expected to be completely damaged before shear damage occurs. When comparing the vulnerability of the isolators on the piers (Fig. 11g) to the isolators of the abutment (Fig. 11h), two observations can be made: (i) the isolators upstream on the piers are under tension, whilst the isolators downstream on the abutments suffer from tensile stress, (ii) the bearings on the scoured pier are more prone to failure by tension than the bearings on the adjacent abutment.

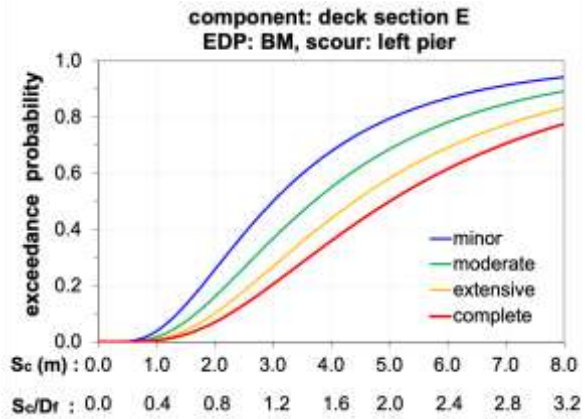
Table 3. Parameters of fragility curves for the critical components of a three-span bridge (integral or with bearings) with shallow foundations, exposed to flood effects (scour, debris and hydraulic forces).

							
component	damage state	median IM [m]	β_{tot}	median IM [m]	β_{tot}		
(1)	(2)	(3)	(4)	(5)	(6)		
integral bridge	deck section F/A/B/H/E (as per Figure 4)	minor moderate extensive complete	3.4/3.5/1.1/4.5/2.7 4.0/4.7/3.1/5.8/3.5 4.6/6.2/5.5/7.3/4.4 5.1/7.5/8.3/8.6/5.2	0.64/0.55/1.0/0.56 /0.58	3.3/-*/3.5/3.4/2.9 3.6/-/4.9/3.7/5.2 3.9/-/6.0/4.0/6.5 4.2/-/7.0/4.2/7.6	0.69/- /1.0/0.68/1.02	
	pier foundation (p1)	minor moderate extensive complete	3.5 4.7 6.5 7.6	0.87	3.4 4.6 6.4 7.4	0.92	
	abutment (a1/a2) EDP: BM	minor moderate extensive complete	5.5/- 6.4/- 7.1/- 7.6/-	0.64/-	4.3/4.3 4.6/4.6 4.9/4.9 5.1/5.1	0.70/0.70	
	deck section A/B/H/E (as per Figure 4)	minor moderate extensive complete	3.5/3.3/5.2/3.0 4.2/3.7/6.3/3.7 5.0/4.0/7.5/4.4 5.6/4.2/-/5.0	0.63/0.62/0.62/ 0.62	3.6/3.1/3.8/3.1 4.0/3.4/4.1/3.4 4.6/3.6/4.3/3.6 5.0/3.7/4.5/3.7	0.80/0.61/1.17 /0.60	
	pier foundation (p1)	minor moderate extensive complete	2.7 3.1 3.7 4.0	1.00	2.8 3.1 3.4 3.6	1.35	
	a1 bearings (shear/ compr@1/ tension@4)	minor moderate extensive complete	2.4/6.4/4.5 3.3/-/5.0 4.9/-/5.6 6.7/-/6.3	0.50/0.37/0.40	2.3/3.6/3.7 3.1/5.5/4.7 4.4/7.0/6.0 5.7/-/7.6	0.52/0.43/0.83	
	p1 bearings (tension@1/ compr@4)	minor moderate extensive complete	4.1/2.9 4.7/6.2 5.4/- 6.2/-	0.60/0.36	5.1/2.6 6.0/4.7 7.1/6.5 -/-	1.80/0.36	
	p2 bearings (tension@1/ compr@4)	minor moderate extensive complete	-/ -/ -/ -/-	-/-	5.1/2.6 6.1/4.6 7.4/6.5 -/-	1.72/0.36	
	a2 bearings (shear/ compr@1/ tension@4)	minor moderate extensive complete	4.5/-/5.8 6.0/-/6.4 -/-/7.1 -/-/7.8	0.50/-/0.70	2.6/3.6/3.7 3.3/5.5/4.7 4.5/-/6.0 5.6/-/7.6	0.55/0.48/0.83	

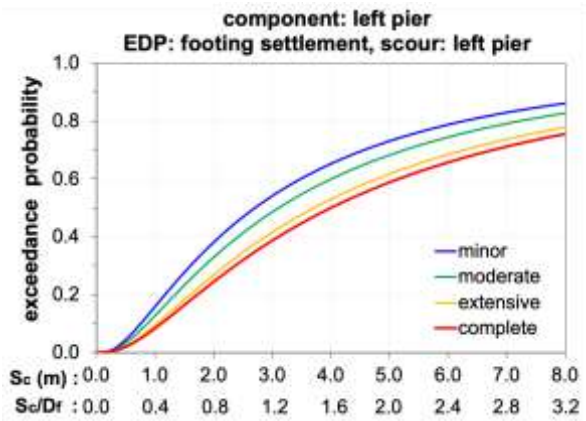
* where no values are given, correspond to cases where the parameters were calculated based on extrapolation of the numerical results, and hence, are not considered reliable or correspond to cases where no damage was observed.



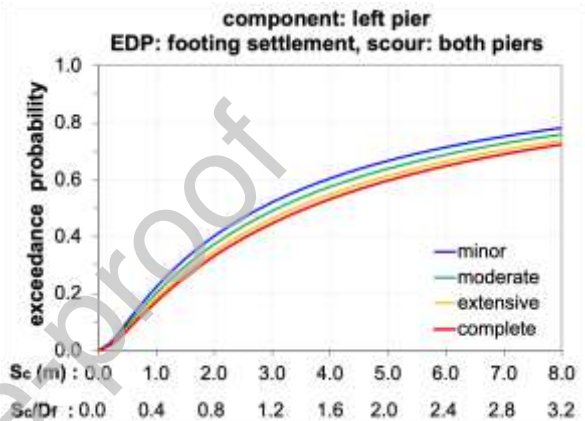
(a)



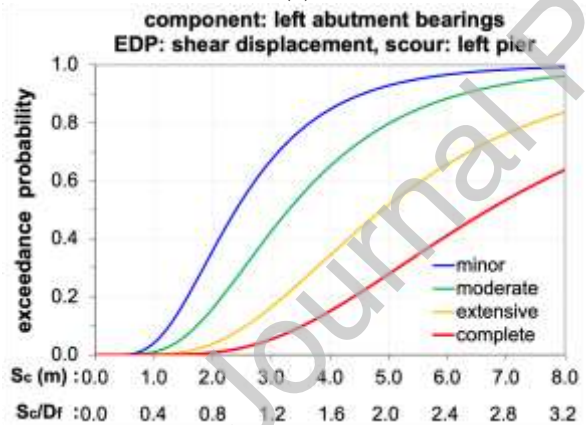
(b)



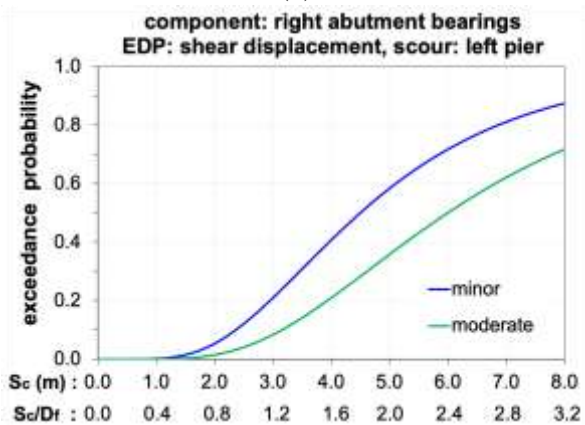
(c)



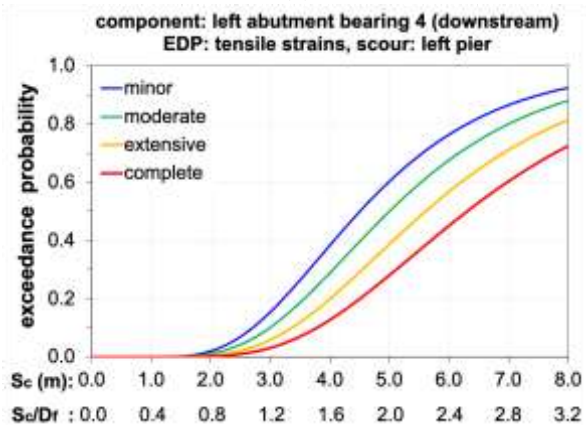
(d)



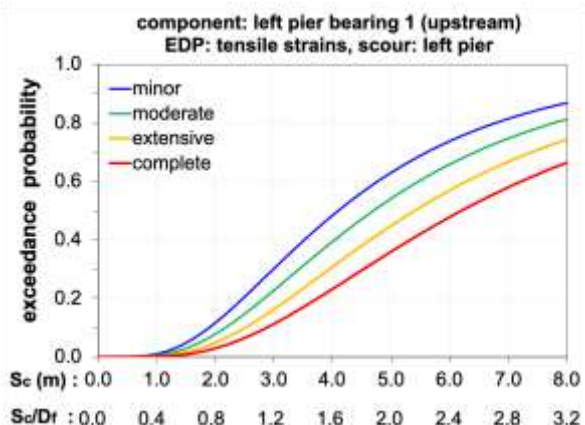
(e)



(f)



(g)



(h)

Figure 11. Fragility curves for the critical components of the bridge with bearings (scour with debris accumulation), as a function of scour depth (S_c) and ratio of scour over foundation depth (S_c/D_f).

Figure 12 shows the **fragility of the system** both for the bridge with bearings and for the integral system, for one and both piers being that are scoured, considering also debris accumulation. The continuous curves correspond to the upper bound, where the system consists of series of fully correlated components, whereas the dashed curves show the fragility of the bridge, where the failure of one component leads to failure of the entire bridge.

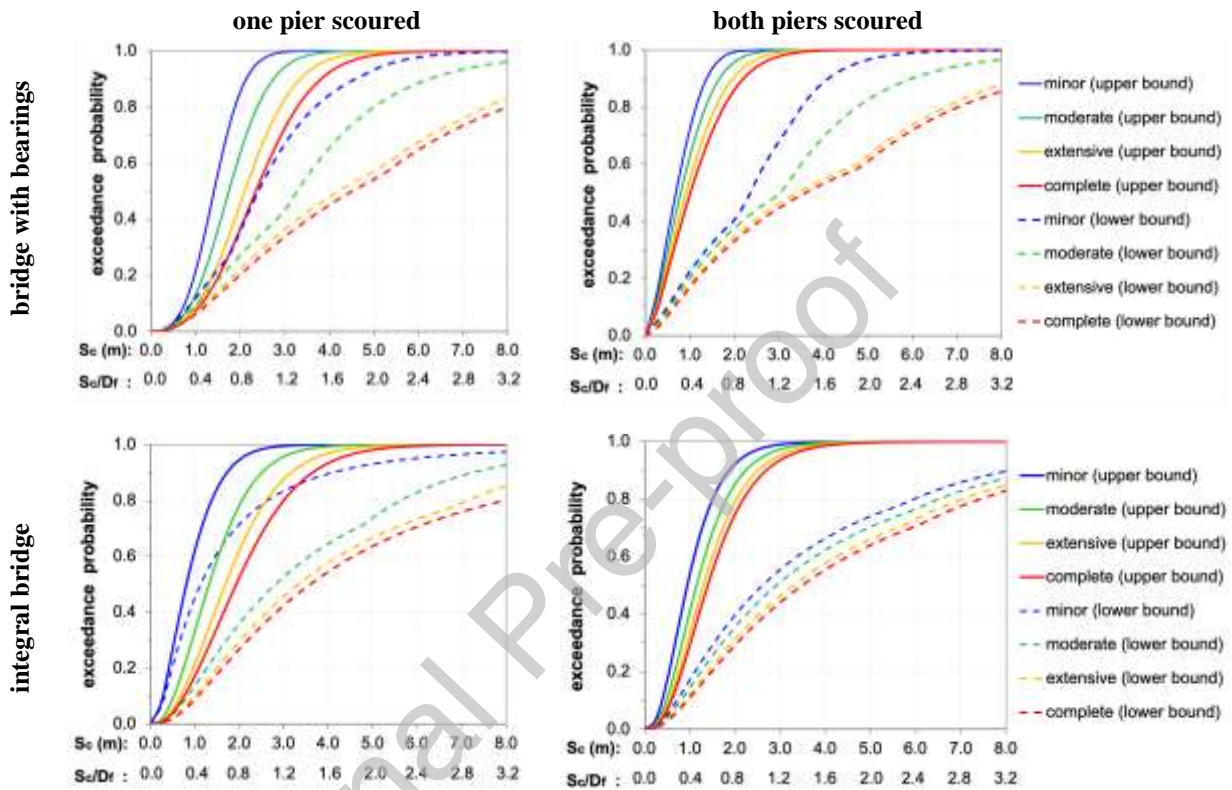


Figure 12. System fragility curves for bridge with bearings (top row) and integral bridge (bottom row) for flood only.

The comparison of the integral with the isolated bridge when local scour occurs at one pier foundation leads to these two observations: (i) although the integral bridge responds with smaller settlements (see Fig. 8), these settlements exert additional stresses, and as a result, integral bridges appear to be more fragile than the isolated ones. This trend is more pronounced in the minor damage state and applies to both the upper and lower bound. (ii) There is a relatively large distance between the fragility curves that illustrate minor and extensive failure, meaning that some warning is expected after the first sign of minor damage. With regard to the abrupt change in the fragility slope of e.g. see lower bound of moderate damage in the bridge with bearings (dashed green curve), it has been found that this is due to the fact that the maximum failure probability is taken from the most vulnerable component, and this is the case where the failure probability of the abutment bearings overtakes that of the piers. These abrupt changes in the slope are not observed in the upper bounds, as these are cumulative probabilities of all component reliabilities. Therefore, the very point of these changes in the curve slope is due to the assumption of series connection between critical components, where excessive damage to one component would lead to significant damage to the entire system (lower bound).

Conversely, the integral bridge appears to be more robust when this scour is generalised, i.e. when the scour occurs on both pier foundations. Again, the failure of bearings is pronounced in the lower bound curves of the

isolated bridge, and defines the minor and moderate failure modes, when the scour depth exceeds 2.0 and 3.0 m, correspondingly. It seems that although at small scour depths the pier settlement defines the highest probability of failure, the bearings become more critical at larger scour depths. For this reason, none of the integral bridge fragility curves resulted in abrupt changes in their slopes.

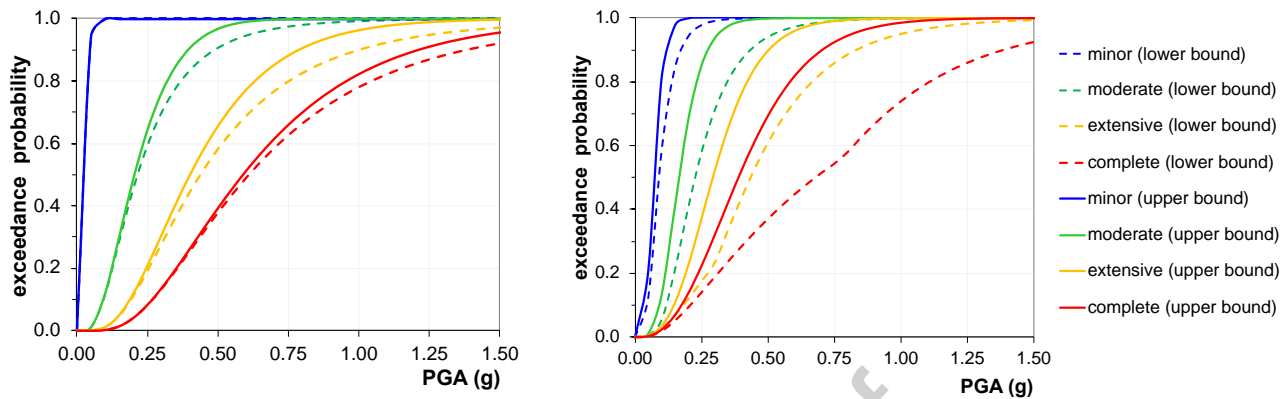


Figure 13. Multihazard system fragility curves for bridge with bearings (left) and integral bridge (right) exposed to one pier scour of $1.5D_f$ followed by earthquake (EQ).

Similar to the fragility curves that were generated for one hazard, i.e. flooding, sets of fragility curves were also generated for multihazard scenarios. The stressors of flood-induced scour followed by earthquakes were considered. Figure 13 illustrates the bridge system fragility models for a scour depth of $1.5D_f$, i.e. 3.75 m, and for PGA between 0.0 and 1.50 g. Fragility curves and surfaces (see e.g. Fig. 14) were also generated for the different scour depths and individual components of the bridges, considering that the local scour affected either one pier or one abutment. Figure 13 shows that at very small PGA on the bridge with bearings minor damage is attained, but it was found that the integral bridge attains moderate, extensive and complete damage compared to the bridge with bearings at smaller PGAs. The reason for this higher vulnerability of the integral bridge is a sequence of events leading to failure of the abutment, the deck in section E, the backfill and the other pier: (i) in case of negligible to small scour holes, the backfill soil is the main component suffering seismic damage (Argyroudis et al., 2018), (ii) with the enlargement of the scour hole the scoured pier becomes more flexible (Tubaldi et al., 2019; Loli et al., 2018) and thereby, attains smaller bending moments under the horizontal displacements of the deck, (iii) the redundant bending moments of the scoured pier are now attracted by the adjacent abutment and pier, which now suffers damage, (iv) at the same time, the deck is damaged at the position of the support of the adjacent pier. In the isolated bridge, the most critical components appear to be the bearings, whose axial strains change dramatically. As a consequence, it has been observed that the deck and especially section E first and later section A suffer damage, followed by failure of the settling pier foundation, damage in the backfill, the abutment, while the flexural capacity of the unscoured pier is the last resort of the bridge. Slightly different results were observed for greater scour depths, i.e. again the bearings and the deck are the most vulnerable components, followed by the settling pier, whilst the abutment and the backfill soil are the components suffering the least. Further information regarding the fragility of the pier and the abutment for combined hazards (FL and EQ), e.g. the abutment or the pier are scoured, is shown in Figure 14.

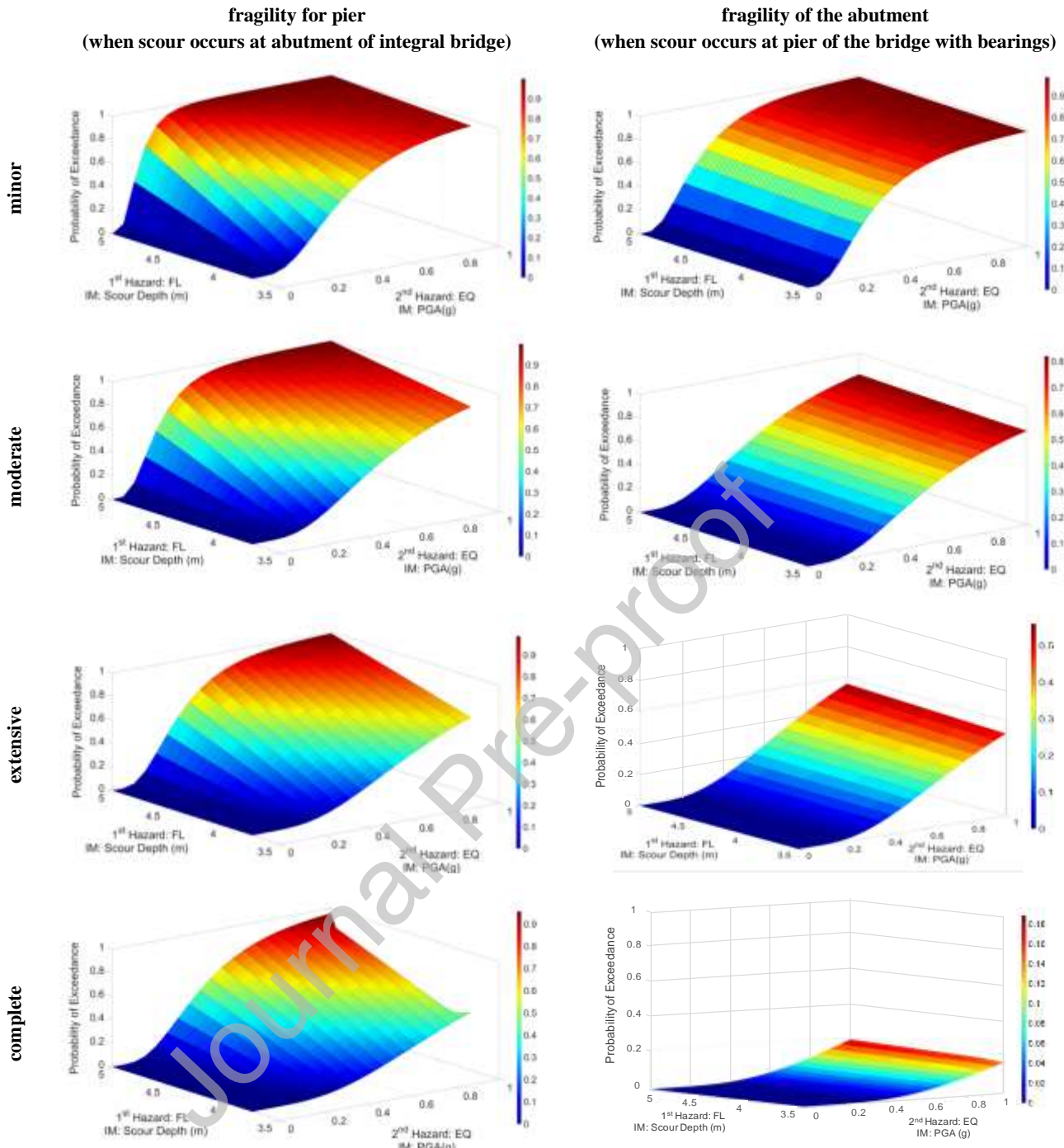


Figure 14. Fragility surfaces for the pier (left column) and the abutment (right column) exposed to FL induced scour and EQ (foundation depth $D_f = 2.5\text{m}$).

The abutment shown in Figure 14 (right column) has low probability of failure as it is independent from the settling pier thanks to the bearings, which do not allow the propagation of failure to the abutment, as well as to the high capacity of the latter. This further strengthens the argument that the fragility of the bridge with bearings heavily depends on the fragility of the bearings and the pier when the latter settles. Yet, there are cases, where failure probabilities are high for high level of scour even for negligible PGA levels. For example, Figure 15, shows the fragility surfaces for the scoured pier of the integral bridge exposed to a combination of flood induced scour and earthquake. By comparing Figure 15 with Figure 14 (left column), it is extracted that the pier is much more vulnerable when scour occurs at its foundation as opposed to having scour formed at

the foundation of the adjacent abutment. Note that for FL only, Table 3 should be used instead of Figures 14 and 15, because a more accurate 3D model was employed for FL only, and hence more representatives EDPs were considered. For example, a pier settling due to scour may not exhibit flexural failures, yet, large dislocations of the pier render it ineffective, i.e. it is not serving its purpose to support the deck. Thus, the dislocation displacement is more appropriate in this occurrence. Figures 14 and 15 are more appropriate for combinations of hazards.

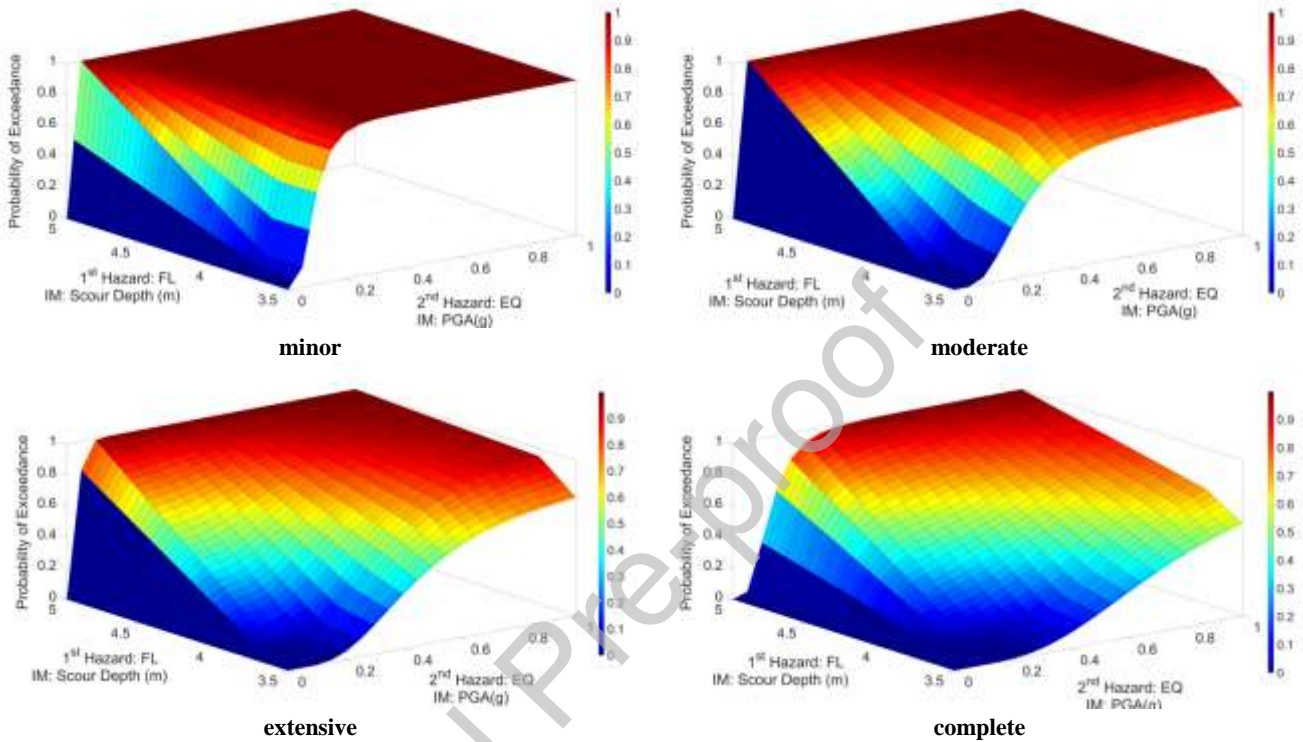


Figure 15. Fragility surfaces for the scoured pier of the integral bridge exposed to a combination of FL induced scour and EQ (foundation depth $D_f = 2.5\text{m}$).

6. Conclusions

In this paper, new fragility models for flood-critical bridges were generated for single hazards (flood) and combined hazards (flood-earthquake). These fragility models are accordingly represented either by curves or surfaces. The main novelty of this research is the analysis of shallow foundations with validated 3D numerical models, considering the full interaction and compatibility of the failure modes of foundation, soil, bridge and backfill, both for integral and isolated bridges, i.e. with bearings. Flooding effects included the main stressors, i.e. global and local scour, debris accumulation and hydraulic forces. Diverse realistic scour hole geometries and their locations were examined to increase the reliability of the fragility functions. Typical ranges of intensity measures were considered to cover practical flood and earthquake scenarios. Therefore, scour hole depths up to twice the depth of foundation and peak ground accelerations up to 0.6 g were analysed. Subsequently, the fragility was evaluated for the components, i.e. deck, bearings, piers, abutments, backfill and for the entire bridge.

The comparison of the flood fragility of the bridge without bearings (integral) to the one with bearings (isolated), showed that in case of scour formation at one pier foundation, the integral bridge is more vulnerable. With regard to the fragility of the individual component, it was found that in the case of the integral bridge, the deck section at the scoured pier is most vulnerable, followed by the deck section at the

adjacent pier. For the isolated bridge, the abutment bearings are the most vulnerable components, followed by the scoured pier. This is based on the range of median values of component fragilities. It seems therefore that vertically flexible systems with bearings that can absorb settlements are more resilient, both because the vulnerability is lower and the restoration can be faster by replacing the damaged components, e.g. the bearings. In the case of global scour, i.e. both piers are in the riverbed and are scoured, the same deck sections of the abovementioned integral bridge and the bearings at the adjacent abutment and the scoured pier in the isolated, are the first components to attain damage. Overall, integral bridges proved to be more robust when both piers are scoured than their isolated counterparts, contrary to the result obtained for more localised effects, i.e. scour at one pier. For earthquakes after flood-induced scour holes with a depth of $1.5D_f$ on one pier, the isolated bridge also seems to withstand the stressors more efficiently, at least in comparison to the integral bridge in the case of moderate, extensive and complete damage, although the bridge with bearings attained slight damage at smaller PGAs. However, at lower scour depths (0 to $1D_f$), the integral bridge appears to be more robust, as the backfill soil acts as external support. At greater scour depths ($2D_f$), the integral bridge was again found to be less vulnerable, as the piers and the abutments retained their capacities and can withstand seismic actions, whereas in the case of the isolated bridge the piers have already failed resulting in complete damage to the bridge.

The significance and practicality of this research is that it enables reliable risk assessments for network owners and operators to quantify the performance and losses to be expected from single or multiple hazards on bridges. This advancement is of interest to both designers and assessors, who evaluate the performance of transport assets throughout their lifecycle. The latter is of paramount importance for decision making, for prioritising and informing interventions proactively to the hazard occurrences, e.g. adaptation to climate change, and/or reactively after the hazard events. In this respect, the infrastructure owners can evaluate the expected damage, the corresponding economic losses and the reduction of the functionality of the assets for different hazard scenarios. In extension, owners can assess and project the impact of hazards on the local network to quantify the resilience to natural and climatic stressors, at a regional and national level.

Acknowledgements

This research has received funding from the H2020 Marie Skłodowska-Curie-IF, Grant Agreement No746298 (Project TRANSRISK). The authors would also like to acknowledge the help provided by seven students of the University of Surrey (alphabetically): Luther Blankson, Alexandru Guja, Roman Omar, Pamela E Samson, Alec Smith, Max Woolcott and Vincent L.F. Yuan.

Authors statement

Sotirios A Argyroudis: Conceptualisation, Methodology, Validation, Formal analysis, Investigation, Resources, Writing - Original Draft, Writing - Review & Editing, Visualization, Funding acquisition. **Stergios Aristoteles Mitoulis:** Conceptualisation, Methodology, Validation, Formal analysis, Investigation, Resources, Writing - Original Draft, Writing - Review & Editing, Visualization.

Conflict of interest

None

References

Achillopoulou DV, Mitoulis SA, Argyroudis SA, Wang Y. Monitoring of transport infrastructure exposed to multiple hazards: A roadmap for building resilience. *Science of the Total Environment* 2020;746:141001.

- Ahamed T, Duan JG, Jo H. Flood-fragility analysis of instream bridges—consideration of flow hydraulics, geotechnical uncertainties, and variable scour depth. *Structure and Infrastructure Engineering* 2020; <https://doi.org/10.1080/15732479.2020.1815226>
- Akiyama M, Frangopol DM, Ishibashi H. Toward life-cycle reliability-, risk-and resilience-based design and assessment of bridges and bridge networks under independent and interacting hazards: emphasis on earthquake, tsunami and corrosion. *Structure and Infrastructure Engineering* 2019; <https://doi.org/10.1080/15732479.2019.1604770>
- Argyroudis S, Kaynia AM. Analytical seismic fragility functions for highway and railway embankments and cuts. *Earthquake Engineering and Structural Dynamics* 2015; 44(11):1863–1879.
- Argyroudis S, Mitoulis SA, Winter MG, Kaynia AM. Fragility of transport assets exposed to multiple hazards: State-of-the-art review toward infrastructural resilience. *Reliab Eng Syst Saf* 2019;191:106567.
- Argyroudis SA, Mitoulis SA, Hofer L, Zanini MA, Tubaldi E, Frangopol DM. Resilience assessment framework for critical infrastructure in a multi-hazard environment. *Science of the Total Environment* 2020a; 714:136854.
- Argyroudis SA, Nasiopoulos G, Mantadakis N, Mitoulis SA. Cost-based resilience assessment of bridges subjected to earthquakes. *International Journal of Disaster Resilience in the Built Environment* 2020b; DOI 10.1108/IJDRBE-02-2020-0014.
- Argyroudis S, Mitoulis S, Kaynia AM, Winter MG. Fragility assessment of transportation infrastructure systems subjected to earthquakes. *Proceedings GEESD V, Geotechnical Special Publication (GSP 292)*. 2018.
- Arneson LA, Zevenbergen LW, Lagasse PF, Clopper PE. Evaluating scour at bridges. *Hydraulic Engineering Circular (HEC) No. 18, Publication No. FHWA-HIF-12-003*, Washington, DC, 2012.
- Aydinoglu MN (2004). An improved pushover procedure for engineering practice: Incremental Response Spectrum Analysis (IRSA). In (Eds: P. Fajfar, H. Krawinkler) *Proceedings of the International Workshop “Performance-based seismic design. Concepts and implementation*, PEER Report 2004/05.
- Ayyub BM. Systems resilience for multihazard environments: definition, metrics, and valuation for decision making. *Risk Analysis* 2014;34(2):340-355.
- Banerjee S, Prasad GG. Seismic risk assessment of reinforced concrete bridges in flood-prone regions. *Structure and Infrastructure Engineering* 2013;9:952–968.
- Banerjee S, Vishwanath BS, Devendiran DK. Multihazard resilience of highway bridges and bridge networks: a review. *Structure and Infrastructure Engineering* 2019;15(12):1694-1714.
- BD97/12. Design manual for roads and bridges: Vol. 3: highway structures: inspection and maintenance, section 4: assessment, part 21: the assessment other hydraulic actions at highway structures. UK: The Highways Agency; 2012.
- Billah AHM, Alam MS. Seismic fragility assessment of highway bridges: a state-of-the-art review. *Structure and Infrastructure Engineering* 2015;11(6):804-832.
- Briaud JL. Scour depth at bridges: method including soil properties. I: maximum scour depth prediction. *Journal of Geotechnical and Geoenvironmental Engineering* 2015;41(2), DOI: 10.1061/(ASCE)GT.1943-5606.0001222.
- Briaud JL, Gardoni P, Yao C. Statistical, risk, and reliability analyses of bridge scour. *Journal of Geotechnical and Geoenvironmental Engineering* 2014;140(2):04013011.
- Bruneau M, Barbato M, Padgett J, Zaghi AE, Mitrani-Reiser J, Li Y. State of the art of multihazard design. *Journal of Structural Engineering* 2017;143(10):03117002.
- Cook W, Barr PJ, Halling MW. Bridge failure rate. *Journal of Performance of Constructed Facilities* 2015;29(3):04014080.
- Decò A, Bocchini P, Frangopol DM. A probabilistic approach for the prediction of seismic resilience of bridges. *Earthquake Engineering & Structural Dynamics* 2013;42(10):1469-1487.
- Dikanski H, Imam B, Hagen-Zanker A. Effects of uncertain asset stock data on the assessment of climate change risks: A case study of bridge scour in the UK. *Structural Safety* 2018; 71:1-12.
- Dong Y, Frangopol DM, Saydam D. Time-variant sustainability assessment of seismically vulnerable bridges subjected to multiple hazards. *Earthquake Engineering and Structural Dynamics* 2013;42:1451-1467.
- Dong Y, Frangopol DM. Risk and resilience assessment of bridges under mainshock and aftershocks incorporating uncertainties. *Engineering Structures* 2015; 83:198-208.
- EN 1992-1-1. Eurocode 2: Design of concrete structures - Part 1-1: General rules and rules for buildings. Brussels: CEN;2004.
- EN 1998-1. Eurocode 8: Design of structures for earthquake resistance – Part 1: General rules, seismic actions and rules for buildings. Brussels: CEN;2004.

- EN 1991-1-6. Eurocode 1: Actions on structures - Part 1-6: General actions - Actions during execution. sels: CEN;2005.
- Gardoni P, Mosalam KM, Der Kiureghian A. Probabilistic seismic demand models and fragility estimates for RC bridges. *Journal of Earthquake Engineering* 2003;7:79-106.
- Gardoni P, Der Kiureghian A, Mosalam KM. Probabilistic capacity models and fragility estimates for RC columns based on experimental observations. *ASCE Journal of Engineering Mechanics* 2002; 128(10):1024-1038.
- Ghosh J, Padgett JE. Aging considerations in the development of time-dependent seismic fragility curves. *Journal of Structural Engineering* 2010;136(12):1497-1511.
- Ghosh J, Sood P. Consideration of time-evolving capacity distributions and improved degradation models for seismic fragility assessment of aging highway bridges. *Reliability Engineering & System Safety*. 2016; 154:197-218.
- Gidaris I, Padgett JE, Barbosa AR, Chen S, Cox D, Webb B, Cerato A. Multiple hazard fragility and restoration models of highway bridges for regional risk and resilience assessment in the United States: state-of-the-art review. *J Struct Eng* 2017;143(3).
- Guo X, Wu Y, Guo Y. Time-dependent seismic fragility analysis of bridge systems under scour hazard and earthquake loads. *Engineering Structures* 2016;121:52–60.
- Guo X, Badroddin M, Chen Z. Scour-dependent empirical fragility modelling of bridge structures under earthquakes. *Advances in Structural Engineering* 2019;22(6):1384-1398.
- Hardin BO. The nature of stress-strain behavior for soils. *Proceedings of the ASCE Geotechnical Engineering Division Specialty Conference, June 19-21, 1978, Pasadena, California*.
- He H, Wei K, Zhang J, Qin S. Application of endurance time method to seismic fragility evaluation of highway bridges considering scour effect. *Soil Dynamics and Earthquake Engineering* 2020;136:106243.
- Huang W, Xiao H. Numerical modeling of dynamic wave force acting on Escambia Bay Bridge deck during Hurricane Ivan. *Journal of Waterway, Port, Coastal, and Ocean Engineering* 2009;135(4):164-175.
- Hung C, Yau W. Vulnerability evaluation of scoured bridges under floods. *Engineering Structures* 2017;132:288-299.
- IPCC (Intergovernmental Panel on Climate Change). *Climate change 2014: Synthesis report. Contribution of Working Groups I, II, and III to the Fifth Assessment Rep. of the IPCC, Geneva, 151. 2014.*
- Jayaram N, Lin T, Baker JW. A computationally efficient ground-motion selection algorithm for matching a target response spectrum mean and variance. *Earthquake Spectra* 2011; 27(3):797-815.
- Kameshwar S, Padgett JE. Multi-hazard risk assessment of highway bridges subjected to earthquake and hurricane hazards. *Engineering Structures* 2014;78:154-166.
- Karamlou A, Bocchini P. Computation of bridge seismic fragility by large-scale simulation for probabilistic resilience analysis. *Earthquake Engineering & Structural Dynamics* 2015;44(12):1959-1978.
- Kelly JM, Konstantinidis D. *Mechanics of rubber bearings for seismic and vibration isolation*. John Wiley & Sons, 2011. DOI:10.1002/9781119971870
- Kim H, Sim SH, Lee J, Lee YJ, Kim JM. Flood fragility analysis for bridges with multiple failure modes. *Advances in Mechanical Engineering* 2017;9(3), <https://doi.org/10.1177/1687814017696415>
- Kim SH, Shinozuka M. Development of fragility curves of bridges retrofitted by column jacketing. *Probabilistic Engineering Mechanics* 2004;19(1-2):105-112.
- Koks EE, Rozenberg J, Zorn C, Tariverdi M, Vousdoulas M, Fraser SA, Hall JW, Hallegatte S. A global multi-hazard risk analysis of road and railway infrastructure assets. *Nature Communications* 2019;10:2677.
- Lamb R, Aspinall W, Odbert H, Wagener T. Vulnerability of bridges to scour: insights from an international expert elicitation workshop. *Nat. Hazards Earth Syst. Sci* 2017;17:1393–1409.
- Lamb R, Garside P, Pant R, Hall JW. A probabilistic model of the economic risk to Britain's railway network from bridge scour during floods. *Risk Analysis* 2019;39(11):2457-2478.
- Li Y, Ahuja A, Padgett JE. Review of methods to assess, design for, and mitigate multiple hazards. *Journal of Performance of Constructed Facilities* 2011;26(1):104-117.
- Li Y, Dong Y, Frangopol DM, Gautam D. Long-term resilience and loss assessment of highway bridges under multiple natural hazards. *Structure and Infrastructure Engineering* 2020;16(4):626-641.
- Lin C, Han J, Bennett C, Parsons RL. Case history analysis of bridge failures due to scour. *Proceedings of the International Symposium of Climatic Effects on Pavement and Geotechnical Infrastructure, August 4-7, 2013, Fairbanks, Alaska*.
- Liu W, Song Z. Review of studies on the resilience of urban critical infrastructure networks. *Reliability Engineering & System Safety* 2020; 193:106617.

- Loli M, Kourkoulis R, Gazetas G. Physical and numerical modeling of hybrid foundations to mitigate seismic fault rupture effects. *Journal of Geotechnical and Geoenvironmental Engineering* 2018;144(11):04018083.
- Lounis Z, McAllister TP. Risk-based decision making for sustainable and resilient infrastructure systems. *Journal of Structural Engineering* 2016;142(9):F4016005.
- Mathews R, Hardman M. Lessons learnt from the December 2015 flood event in Cumbria, UK. *Proceedings of the Institution of Civil Engineers-Forensic Engineering* 2017;170(4):165-178.
- May RWP, Ackers JC, Kirby AM. *Manual on scour at bridges and other hydraulic structures*, C551, CIRIA, London, 2002.
- McKenna G, Argyroudis SA, Winter MG, Mitoulis SA. Multiple hazard fragility analysis for granular highway embankments: moisture ingress and scour. *Transportation Geotechnics* 2020;26:100431, <https://doi.org/10.1016/j.trgeo.2020.100431>.
- Mitoulis SA. Challenges and opportunities for the application of integral abutment bridges in earthquake-prone areas: A review. *Soil Dynamics and Earthquake Engineering* 2020;135:106183.
- Mitoulis SA. Uplift of elastomeric bearings in isolated bridges subjected to longitudinal seismic excitations. *Structure and Infrastructure Engineering* 2015;11(12):1600-1615.
- Mitoulis SA, Argyroudis S, Loli M, Imam B. Restoration models for quantifying flood resilience of bridges. *Engineering Structures* 2021 (accepted).
- Mondoro A, Frangopol DM, Liu L. Bridge adaptation and management under climate change uncertainties: A review. *Natural Hazards Review* 2018;19(1):04017023.
- Nasr A, Björnsson I, Honfi D, Larsson Ivanov O, Johansson J, Kjelstrom E. A review of the potential impacts of climate change on the safety and performance of bridges. *Sustainable and Resilient Infrastructure* 2019;31:1-21.
- Nasr A, Kjellström E, Björnsson I, Honfi D, Ivanov OL, Johansson J. Bridges in a changing climate: a study of the potential impacts of climate change on bridges and their possible adaptations. *Structure and Infrastructure Engineering* 2020;16(4):738-749.
- Nielson B, DesRoches R. Analytical seismic fragility curves for typical highway bridge classes in the central and Southeastern United States. *Earthquake Spectra* 2007;23(3):615–633.
- Nofal O, van de Lindt JW, Do TQ. Multi-variate and single-variable flood fragility and loss approaches for wood frame buildings. *Reliability Engineering & System Safety* 2020; 106971.
- Panici D, de Almeida GA. Formation, growth, and failure of debris jams at bridge piers. *Water Resources Research* 2018; 54(9):6226-6241.
- Panici D, de Almeida GA. Influence of pier geometry and debris characteristics on wood debris accumulations at bridge piers. *Journal of Hydraulic Engineering* 2020;146(6):04020041.
- Panici D, Kripakaran P, Djordjević S, Dentith K. A practical method to assess risks from large wood debris accumulations at bridge piers. *Science of The Total Environment* 2020;728:138575.
- Pizarro A, Ettmer B, Manfreda S, Rojas A, Link O. Dimensionless effective flow work for estimation of pier scour caused by flood waves. *Journal of Hydraulic Engineering* 2017;143(7):06017006.
- Pizarro A, Manfreda S, Tubaldi E. The science behind scour at bridge foundations: A review. *Water* 2020;12(2):374.
- Plaxis 3D. Reference Manual, in *Plaxis 3D User's Manual*. 2019.
- Prasad GG, Banerjee S. The impact of flood-induced scour on seismic fragility characteristics of bridges, *J Earth Eng* 2013;17:803-828.
- Pregolato M. Bridge safety is not for granted—a novel approach to bridge management. *Engineering Structures* 2019;196: 109193.
- Scozzese F, Ragni L, Tubaldi E, Gara F. Modal properties variation and collapse assessment of masonry arch bridges under scour action. *Engineering Structures* 2019;199: 109665. [10.1016/j.engstruct.2019.109665](https://doi.org/10.1016/j.engstruct.2019.109665)
- Shekhar S, Ghosh J. A metamodeling based seismic life-cycle cost assessment framework for highway bridge structures. *Reliability Engineering & System Safety* 2020; 195:106724.
- Stefanidou S, Kappos A. Bridge-specific fragility analysis: when is it really necessary? *Bulletin of Earthquake Engineering* 2019;17(4):2245-2280, <https://doi.org/10.1007/s10518-018-00525-9>.
- Stefanidou SP, Kappos AJ. Methodology for the development of bridge-specific fragility curves. *Earthquake Engineering Structural Dynamics* 2017; 46(1):73-93.
- Tanasic N, Hajdin R. Management of bridges with shallow foundations exposed to local scour. *Structure and Infrastructure Engineering* 2018;14(4):468-476, doi.org/10.1080/15732479.2017.1406960

- Tsionis G, Fardis MN. Fragility functions of road and railway bridges. In: Ptilakis K, Crowley H, Kaynia AM, editors. SYNER-G: typology definition and fragility functions for physical elements at seismic risk. Springer Netherlands; 2014. Geotechnical, Geological and Earthquake Engineering 27.
- Tubaldi E, Macorini L, Izzuddin BA, Manes C, Laio F. A framework for probabilistic assessment of clear-water scour around bridge piers. *Structural Safety* 2017;69:11–22.
- Tubaldi E, Lupo R, Mitoulis S, Argyroudis S, Gara F. Field tests on a soil-foundation-structure system subjected to scour. Field tests on a soil-foundation-structure system subjected to scour. *Proceedings ANIDIS-XVIII*, 15-19 Sept., Italian National Association of Earthquake Engineering. 2019.
- Vousdoukas MI, Mentaschi L, Voukouvalas E, Verlaan M, Jevrejeva S, Jackson LP, Feyen L. Global probabilistic projections of extreme sea levels show intensification of coastal flood hazard. *Nat Communications* 2018;9(1):1-12.
- Wang Z, Dueñas-Osorio L, Padgett JE. Influence of scour effects on the seismic response of reinforced concrete bridges. *Engineering Structures* 2014;76:202-14.
- Wardhana K, Hadipriono FC. Analysis of recent bridge failures in the United States. *Journal of Performance of Constructed Facilities* 2003;17(3):144-150
- Woods DD. Four concepts for resilience and the implications for the future of resilience engineering. *Reliab Eng Syst Saf* 2015;141:5-9.
- Yilmaz T, Banerjee S, Johnson PA. Performance of two real-life California bridges under regional natural hazards. *Journal of Bridge Engineering* 2016;21(3).
- Zampieri P, Zanini MA, Faleschini F, Hofer L, Pellegrino C. Failure analysis of masonry arch bridges subject to local pier scour. *Engineering Failure Analysis* 2017;79:371-384.
- Zekkos D, Zalachoris G, Alvertos AE, Aatya PM, Blunts P, Clark M, Dafis S, Farmakis I, Ganas A, Hille M, Kalimogiannis V, Karagiannidis A, Karantanellis E, Khan K, Kirshbaum D, Kourkoulis R, Kotroni V, Ktenidou O-J, Lagouvardos K, Loli M, Makrinikas A, Marinos V, Manousakis J, Nikas K, Panousis D, Papathanassiou G, Saroglou C, Simopoulos A, Stanley T, Tsavalas A, Valkaniotis S. The September 18-20 2020 Medicane Ianos Impact on Greece - Phase I Reconnaissance Report. *Geotechnical Extreme Events Reconnaissance Report*, GEER-068, <https://doi.org/10.18118/G6MT1T>.